

UNIVERSITÄTSKLINIKUM HAMBURG-EPPENDORF

Institut für Anatomie II:

Experimentelle Morphologie

Institutsdirektor: Prof. Udo Schumacher

Morphological characterization of Estrogen-Related Receptor γ deficient mice

Dissertation

zur Erlangung des Grades eines Doktors der Medizin
an der Medizinischen Fakultät der Universität Hamburg.

vorgelegt von:

Christos Ganos
aus Thessaloniki, Griechenland

Hamburg 2010

**Angenommen von der
Medizinischen Fakultät der Universität Hamburg am: 16.07.2010**

**Veröffentlicht mit Genehmigung der
Medizinischen Fakultät der Universität Hamburg.**

Prüfungsausschuss, der/die Vorsitzende: Prof. Dr. U. Schumacher

Prüfungsausschuss, zweite/r Gutachter/in: PD. Dr. U. Borgmeyer

Prüfungsausschuss, dritte/r Gutachter/in: Prof. Dr. A. Münchau

Table of Contents

List of abbreviations.....	5
Problem Definition	7
1. INTRODUCTION.....	8
1.1 The nuclear receptor superfamily.....	8
1.2 The structure of a nuclear receptor	10
1.3 Molecular physiology.....	11
1.4 Orphan nuclear receptors.....	11
1.5 The ERRs.....	13
2. MATERIALS.....	15
3. METHODS.....	17
3.1 Animal Breeding	17
3.2 Histology	18
3.2.1 Tissue preparation	18
3.2.2 Perfusion of postnatal animals	18
3.2.3 Sectioning.....	19
3.3 Data Analysis.....	20
3.3.1 Genotyping	20
3.3.2 Isolation of genomic DNA	20
3.3.3 Restriction digests and gel electrophoresis	20
3.3.4 Blotting.....	20
3.3.5 Preparation of the radioactively labeled probe by random priming.....	21
3.3.6 Hybridization.....	21
3.4 Staining procedures	22
3.4.1 Hematoxylin-Eosin Staining	22
3.4.2 Mounting	22
3.4.3 Nissl-Staining with Cresyl-violet.....	22
3.4.4 Masson-Goldner's trichrome staining.....	22
3.4.5 Kluever-Barrera staining.....	23
3.4.6 Periodic Acid Schiff Reaction (PAS).....	23
3.5 Immunohistological Stainings.....	24
3.5.2 Anti-Tyrosine Hydroxylase (Anti-TH)	24
3.6	26
Morphometric Analysis.....	26
4. RESULTS.....	30
4.1 Determination of the genotypes of the ERR γ used in this study	30
4.1.1 Southern Blotting	30
4.1.3 Genotypic Distribution.....	31
4.2 Demonstration of Adult weight differences between the ERR $\gamma^{+/+}$ and the.....	33
ERR $\gamma^{-/-}$ animals	33
4.3 The determination of the beginning of the ERR $\gamma^{-/-}$ weight reduction compared to the ERR $\gamma^{+/+}$	36

4.4 Demonstration of adult vertex-breech-length differences between the ERRγ^{+/+} and the ERRγ^{-/-} animals	38
4.5 ERRγ^{-/-} mouse growth delay compared to the ERRγ^{+/+} mice.	41
4.6 Neurological Phenotype	43
4.7 Morphology	44
4.7.1 Gross morphology	44
4.8 Histology	48
4.8.1 Immunohistochemical examination of the ERR γ triples.....	50
4.9 Morphometry	52
4.9.1 The ERR γ ^{-/-} has a relative bigger mesencephalic tegmentum compared to the ERR γ ^{+/+} , even though its absolute brain size is reduced	52
5. DISCUSSION	55
Pre- and Post-Natal Development	55
Adult ERRγ knockouts	56
The ERRγ Brain	57
Movement Disorders	58
Gastric Tumors	59
One receptor, one mouse model and so many functions	60
REFERENCES	62
Index of figures	69
Index of Tables	71
Acknowledgment	72
ABSTRACT	73
PERSONAL INFORMATION	74
EIDESSTATLICHE VERSICHERUNG	75

List of abbreviations

AAC2 - acetyl-CoA carboxylase-2 isoform
AF-2 - transcriptional activation function
AMPK - adenine monophosphate-activated protein kinase
ATP - Adenosine-5'-triphosphate
cDNA – cloned DNA
COUPs - chicken ovalbumin upstream stimulators
CTE - carboxy-terminal extension
DAB - 3,3'-diaminobenzidine
DBD - DNA-binding domain
DNA – Deoxyribonucleic acid
EcRs - Ecdysone receptors
ERR γ – Estrogen-related receptor γ
ERR $\gamma^{+/+}$ - Estrogen-related receptor γ wildtype mice
ERR $\gamma^{+/-}$ - Estrogen-related receptor γ heterozygous mice
ERR $\gamma^{-/-}$ - Estrogen-related receptor γ knock out mice
ERRE - ERR response element
Ex – embryonic day x
GFAP – Glial fibrillary acid protein
HNF4 - hepatocyte nuclear factor 4
HREs - hormone response elements
LBD - ligand-binding domain
LKB1 - Serine/threonine kinase 11
LXRs - liver-x receptors
MCD - Malonyl CoA decarboxylase
MFH - massive foveolar hyperplasia
MHRE - multi-hormone-response element
NADH - nicotinamide adenine dinucleotide
Ndufb5 - NADH dehydrogenase (ubiquinone) 1 beta subcomplex, 5
NGFI-B - Nerve growth factor-induced clone B
NF-2 Nuclear erythroid 2 p45-related factor 2
NR5A1/SF-1- Steroidogenic factor 1

NTD - amino-terminal domain
PB – Phosphate-Buffer
PBS – Phosphate-Buffer Saline
PFA – Paraformaldehyde
Pgc-1a - Peroxisome proliferator-activated receptor-gamma coactivator 1alpha
PNR - photoreceptor cell-specific nuclear receptor
PPARs - Peroxisome proliferator-activated receptors
Px – postnatal day x
RARs - Retinoic acid receptors
RORs - retinoid-related receptors
RXRs - Retinoid X receptors
TH – Tyrosine Hydroxylase
TRs - Thyroid hormone receptors
TR2 - Testis receptor
VDRs - Vitamin D receptors

Problem Definition

The family of orphan nuclear receptors comprises ligand-independent intracellular and/or intranuclear transcription factors, which play several roles in basic physiological functions such as cell metabolism, differentiation and growth. In 1998 the so far last orphan nuclear receptor, the estrogen-related receptor (ERR) γ , was identified. In order to achieve a more thorough understanding of the receptor's physiological properties, parallel to its genetic and biomolecular characterization, ERR $\gamma^{-/-}$ mice were generated. The purpose of this thesis will be to analyze the phenotype and the morphological changes induced in the mice by the absence of the ERR γ . For comparison, wildtype (ERR $\gamma^{+/+}$) and heterozygous (ERR $\gamma^{+/-}$) mice will be used as well. In addition to conventional histology, morphometry and immunohistochemistry will be used to characterize the ERR $\gamma^{-/-}$ mice.

1. INTRODUCTION

1.1 The nuclear receptor superfamily

Nuclear receptors are intracellular and/or intranuclear ligand-inducible transcription factors for small lipophilic molecules, such as steroid, thyroid hormones or the active forms of vitamin A and vitamin D, which play salient roles in basic physiological functions concerning cell metabolism, differentiation and growth (1). The first identification of a nuclear receptor was made in the year 1962 by Jensen et al. who demonstrated, that estradiol's cellular activity is mediated through a high affinity receptor (2). Since then more than 50 nuclear receptors have been identified in various species, only half of which are liganded (3). The other half of these receptors, for which no regulatory ligands have been identified at yet have been named "orphan nuclear receptors".

Based on evolutionary analysis the nuclear receptor family has been divided to six different subfamilies (4, 5).

1. Thyroid hormone receptors (TRs), Retinoic acid receptors (RARs), Peroxisome proliferator-activated receptors (PPARs), Vitamin D receptors (VDRs), Ecdysone receptors (EcRs) and numerous orphan receptors such as the retinoid-related receptors (RORs) and the liver-x receptors (LXRs).
2. Retinoid X receptors (RXRs) with chicken ovalbumin upstream stimulators (COUPs), hepatocyte nuclear factor 4 (HNF4), testis receptors (TR2) and receptors involved in eye development (TLX and PNR).
3. Steroid receptors and the highly related estrogen-related receptors (ERRs).
4. Nerve growth factor-induced clone B group of orphan receptors [NGFI-B, NURR1, NOR1].
5. Steroidogenic factor 1 (NR5A1/SF-1) and the FTZ-1 orphan receptor.
6. GCNF1 orphan receptor.

The complete nuclear receptor family nomenclature as proposed by the nuclear receptors nomenclature committee is demonstrated in Table 1 (see appendix).

Subfamily and Group	NR/Gene	Trivial Names	Accession Number
1A	NR1A1	TR α , c-erbA-1, THRA	M24748
	NR1A2	TR β , c-erbA-2, THRB	X04707
1B	NR1B1	RAR α	X06538
	NR1B2	RAR β , HAP	Y00291
1C	NR1B3	RAR γ , RARD	M57707
	NR1C1	PPAR α	L02932
	NR1C2	PPAR β , NUC1, PPAR δ , FAAR	L07592
1D	NR1C3	PPAR γ	L40904
	NR1D1	REVERB α , EAR1, EAR1A	M24898
	NR1D2	REVERB β , EAR1 β , BD73, RVR, HZF2	L31785
1E	NR1D3	E75	X51548
	NR1E1	E78, DR-78	U01087
1F	NR1F1	ROR α , RZR α	U04897
	NR1F2	ROR β , RZR β	Y08639
	NR1F3	ROR γ , TOR	U16997
	NR1F4	HR3, DHR3, MHR3, GHR3, CNR3, CHR3	M90806
1G	NR1G1	CNR14	U13075
1H	NR1H1	ECR	U13074
	NR1H2	UR, OR-1, NER1, RIP15, LXR β	M74078
1I	NR1H3	RLD1, LXR, LXR α	U07132
	NR1H4	FXR, RIP14, HRR1	U22662
	NR1I1	VDR	U09416
	NR1I2	ONR1, PXR, SXR, BXR	J03258
1J	NR1I3	MB67, CAR1, CAR α	X75163
	NR1I4	CAR2, CAR β	Z30425
1K	NR1J1	DHR96	AF00932
2A	NR1K1	NHR1	U36792
	NR2A1	HNF4	U19360
	NR2A2	HNF4G	X76930
	NR2A3	HNF4B	Z49826
2B	NR2A4	DHNF4, HNF4D	Z49827
	NR2B1	RXRA	U70874
	NR2B2	RXR β , H-2RIIBP, RCoR-1	X52773
	NR2B3	RXRG	M84820
2C	NR2B4	USP, Ultraspiracle, 2C1, CF1	X66225
	NR2C1	TR2, TR2-11	X52591
2D	NR2C2	TR4, TAK1	M29960
	NR2D1	DHR78	L27586
2E	NR2E1	TLL, TLX, XTLL	U36791
	NR2E2	TLL, Tailless	S72373
2F	NR2F1	COUP-TF1, COUPTFA, EAR3, SVP44	M34639
	NR2F2	COUP-TFII, COUPTFB, ARP1, SVP40	X12795
	NR2F3	SVP, COUP-TF	M64497
	NR2F4	COUP-TFIII, COUPTFG	M28863
	NR2F5	SVP46	X63092
	NR2F6	EAR2	X70300
	NR3A1	ER α	X12794
	NR3A2	ER β	X03635
3B	NR3B1	ERR1, ERR α	U57439
	NR3B2	ERR2, ERR β	X51416
3C	NR3C1	GR	X51417
	NR3C2	MR	X03225
	NR3C3	PR	M16801
	NR3C4	AR	M15716
4A	NR4A1	NGFIB, TR3, N10, NUR77, NAK1	M20132
	NR4A2	NURR1, NOT, RNR1, HZF-3, TINOR	L13740
	NR4A3	NOR1, MINOR	X75918
	NR4A4	DHR38, NGFIB, CNR8, C48D5	D38530
5A	NR5A1	SF1, ELP, FTZ-F1, AD4BP	U36762
	NR5A2	LRH1, xFF1rA, xFF1rB, FFLR, PHR, FTF	U13076
5B	NR5A3	FTZ-F1	D88155
6A	NR5B1	DHR39, FTZF1B	U93553
6A	NR6A1	GCNF1, RTR	M63711
0A	NR0A1	KNI, Knirps	L06423
	NR0A2	KNRL, Knirps related	U14666
0B	NR0A3	EGON, Embryonic gonad, EAGLE	X13331
	NR0A4	ODR7	X14153
	NR0A5	Trithorax	X16631
	NR0B1	DAX1, AHCH	U16708
	NR0B2	SHP	M31617
			S74720
			L76571

Table 1 A proposed nomenclature for the nuclear receptors. [Table from “A unified nomenclature system for the nuclear receptor superfamily” (4)]

Whether these receptors evolved from ancestral constitutive homodimeric transcription factors and acquired the ability to bind to a ligand and to homodimerize or whether they derived from a ligand-dependent receptor, which through mutations changed or lost its ligand-binding specificity remains uncertain (5).

1.2 The structure of a nuclear receptor

The main structural parts of a nuclear receptor consist of:

i. AB domain

The amino-terminal domain (NTD) (A/B domain), which is a variable and unstructured region that can contain an autonomous transcriptional activation function (AF-1), that contributes to ligand-independent activation by the receptor.

ii. C domain

The DNA-binding domain (DBD) (C domain), which is the most conserved domain of nuclear receptors and through which the recognition of short DNA sequences, referred to as hormone response elements (HREs) is achieved resulting in gene activation. The DNA-binding could be obtained through monomeric, homodimeric or heterodimeric receptor subunits. The DBD is composed of two zinc fingers and a carboxy-terminal extension (CTE).

iii. D domain

The hinge region (D domain), which is variably conserved bridging the DBD and the ligand-binding domain (LBD) and allowing rotation of the DBD.

iv. E domain

The LBD (E domain), which through ligand binding mediates homo- and heterodimerization of the receptor and ligand-dependent transcriptional activity or repression. The transcriptional activation function (AF-2), a well-conserved, ligand-dependent domain is contained in this receptor part.

v. F domain

The C-terminal (F domain), which is not consistently present in all nuclear receptors and to which no specific role has been assigned yet.

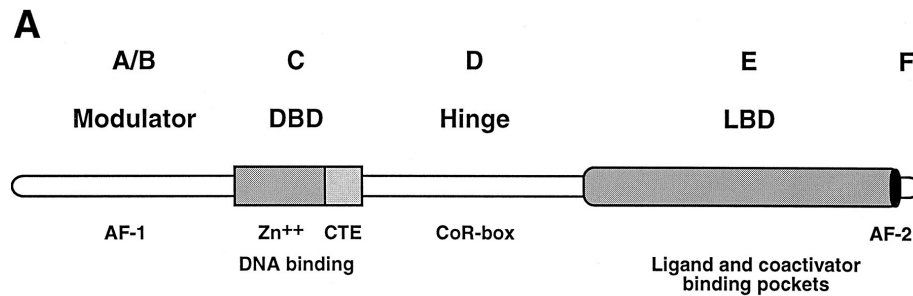


Fig. 1 Anatomy of nuclear receptors. The amino-terminal domain (A/B) domain, that contributes to ligand-independent activation of the receptor. The DNA-binding (C) domain, which leads to gene activation. The hinge region (D domain) bridging the C with the E domain and allowing conformational changes of the receptor. The ligand binding (E) domain through which homo- or hetero-dimerization after ligand binding is achieved and transcriptional activation or suppression is accomplished. The inconsistently appearing in some of the nuclear receptors C-terminal, (F domain), whose function is yet not fully understood. For information see text. [modified from Giguere (6)]

1.3 Molecular physiology

As mentioned above, nuclear receptors can be either cytoplasmic or nuclear in their location (6). Most receptors are constitutively nuclear and in the absence of a ligand are bound to DNA acting as strong transcriptional repressors (6-12). Upon ligand binding the repressor complex dissociates from the receptor, which can then act freely with the coactivator complex leading to chromatin state changes (13). The DNA binding is achieved by the nuclear receptors either as monomers, homodimers or heterodimers (14).

1.4 Orphan nuclear receptors

Where do these orphan receptors come from?

In order to understand the structure and function of the nuclear receptors, biochemical and cloning experiments were conducted showing that these receptors share extensive homology at their nucleotide and amino acid sequence. By using low-stringency screening of cDNA libraries with DBD as probes (“reverse endocrinology”), it was revealed that multiple isoforms can exist for the same ligand, and also that for a series

of proteins with the structural features of a receptor no natural ligand could be identified immediately. These new members of the nuclear receptor family were named “orphan”, the first of which was the estrogen-related receptor alpha in the year 1988 by the group of Giguere and Evans (16).

Table 2 summarizes the identified to date orphan nuclear receptors.

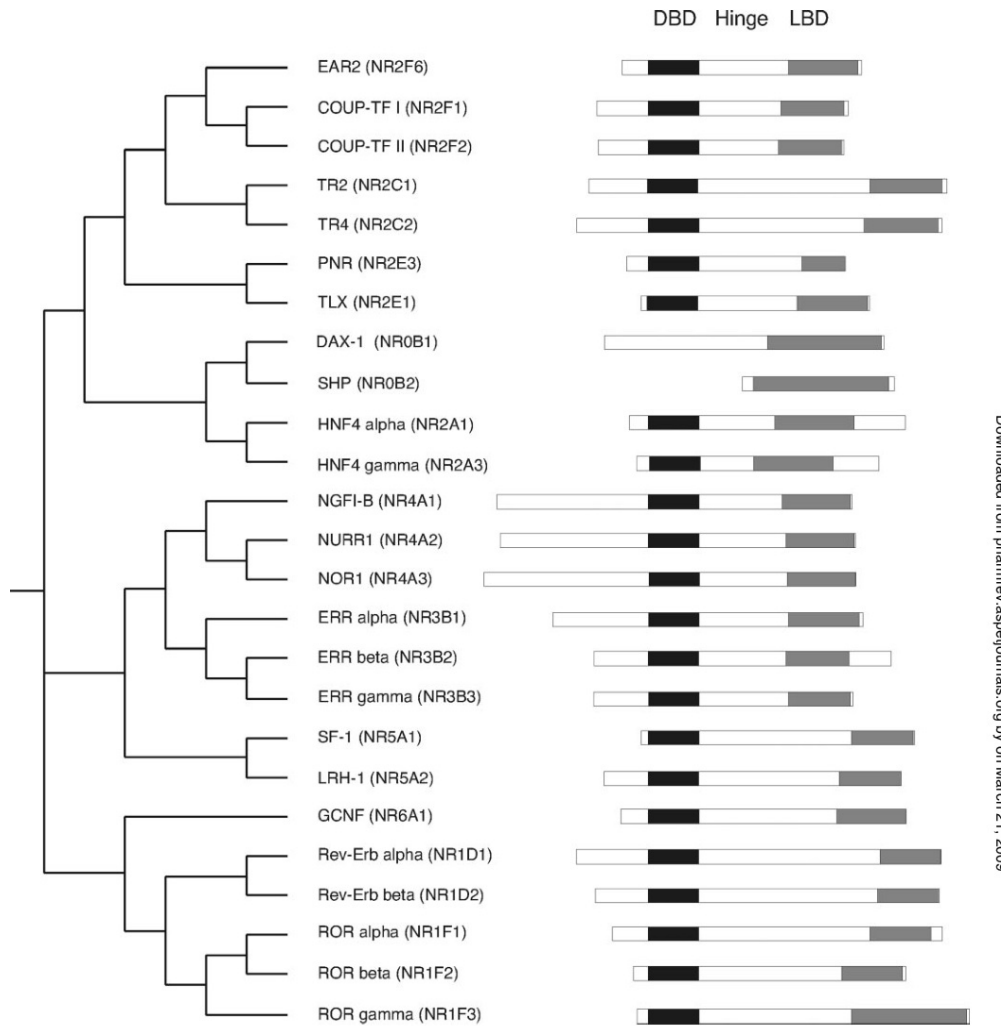


FIG. 1. Phylogenetic tree and schematic structure of orphan nuclear receptors present in human, mouse, and rat.

Table 2 Phylogenetic tree and schematic structure of orphan nuclear receptors present in human, mouse and rat [from Benoit et al. (15)]

What do the orphan receptors do?

The functional properties of each of the members of the orphan nuclear family has been a subject of intensified scientific research over the past twenty years and as demonstrated by Giguere (6) they extend from cell differentiation (17- 19), to

neurogenesis, organogenesis [placenta formation (20)] energy (and drug) metabolism, adrenal development, sexual development, circadian rhythm and metabolism (21) and many more. Additionally a regulatory role over the activity of other ligand-binding receptors has been demonstrated for some of the orphan nuclear receptors, such as the COUP-TFs, TR2, and TR4, which have been shown to repress the activation mediated by liganded receptors such as RAR, TR or PPAR (15).

The complex pattern of the relationship between orphan nuclear receptor expression, function and physiology is illustrated in figure 2. [From the work of Bookout et al. (30)].

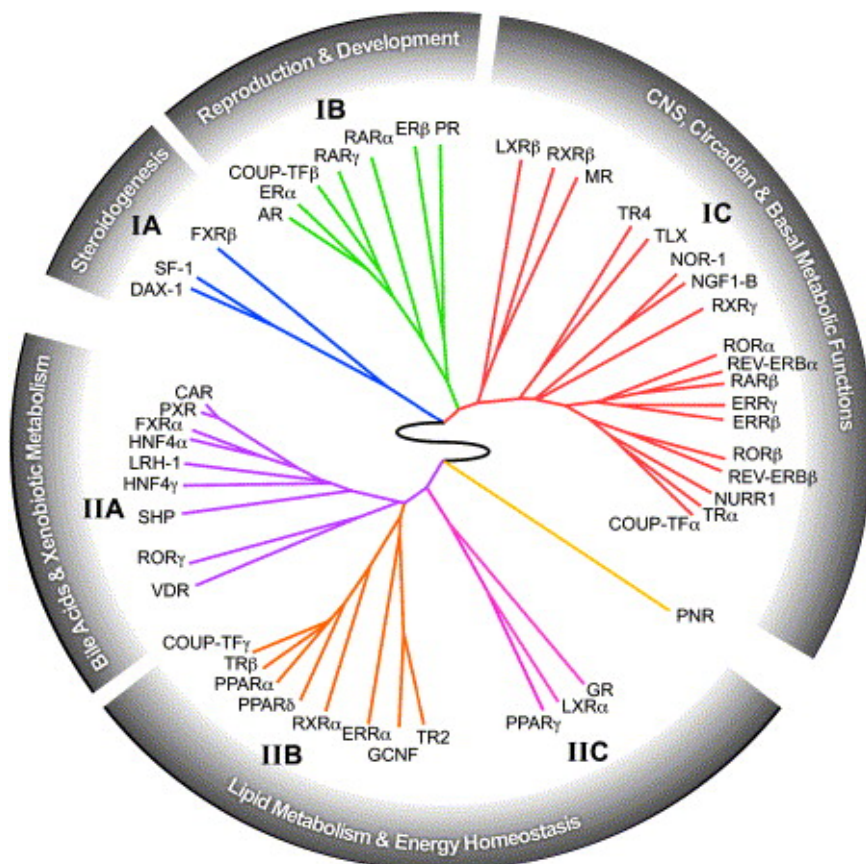


Fig. 2 Circular dendrogram depicting the relationship between nuclear receptor expression, function and physiology, revealing the major role of the nuclear receptors to reproduction, development, central and basal metabolic functions, dietary-lipid-metabolism and energy homeostasis. [from Bookout, A. L., Y. Jeong, et al. (30)].

1.5 The ERRs

The first two estrogen-related receptors (alpha and beta) were identified, as already mentioned above, in the year 1988 during a cDNA search for genes related to the

estrogen receptors (16). Ten years later the third and so far last member of the ERR family (ERR γ) was identified (22-24). This receptor is to date the last orphan nuclear receptor found. Homologs of the ERRs also exist in invertebrates (Drosophila, Amphioxus 25, 26) implying a common ancestry, which has not yet been possible to identify (27).

The expression patterns of the three ERRs are tissue specific, with the ERR α expressed at high levels in tissues with significant energy demands (heart, kidneys) and also in the intestine, brown adipose tissue and skeletal muscles (16, 30). The ERR β is mainly expressed in the developing placenta and in undifferentiated trophoblast stem cell lines (20, 28 – 30). The ERR γ is mainly expressed in the central nervous system (31, 32), heart, kidney and stomach (30).

The combination of biochemical methods and phenotypic analyses of ERR null mice has led to the elucidation of many of the functions of the ERRs, which are summarized at Table 3.

Tissue	Isoform	Function	Prototype target genes
Bone	α	Formation, differentiation	OPN
Breast cancer	α, γ	Prognostic markers, interfere with E2 response	Aromatase; TFF1
Brown adipose	α	Adaptive thermogenesis, mitochondrial biogenesis	IDH3A, CPT-1b
Cartilage	α	Formation and maintenance	Sox9
Heart	α, γ	Bioenergetics, contraction	Atp5b, Ant1, Ckmt2 Casq2, Ldb3, Teap
Inner ear	β	Epithelial cell fate, inner ear fluid homeostasis	KCNQ1, Scl26a4
Intestine	α	Fat transport and absorption	ApoA4
Liver	α	Suppressing gluconeogenesis	PEPCK
Macrophages	α	ROS production, innate immunity	Aco2
Placenta	β	Trophoblast differentiation	?
Skeletal muscle	α	Mitochondria biogenesis, OXPHOS	Cycs, GABPA, ESRRB
White adipose	α	Lipid metabolism	Fasn, Acadm

Table 3 Known ERR functions and associated genes [from Tremblay and Giguere (33)].

2. MATERIALS

Mouse lines:

Estrogen Related Receptor (ERR) – 14

ERR – 33

ERR – 80

C57B1

Chemicals:

- Perfusion

- 4% Paraformaldehyde (PFA)
- 0,1 M Phosphate-Buffer Saline (PBS), pH 7.4
17,8 g Na₂HPO₄ and 16,0 g NaCl ad 1 Liter of distilled water
- 0,2 M Phosphate-Buffer (PB), pH 7.4
28.41g Na₂HPO₄ and 5.52g Na H₂ PO₄ ad 1Liter of distilled water pH 7.4
- Molded Wax – Paraplast
- Ketamin/Rompun – 120mg Ketamin/16mg Rompun in 10ml 0,9% NaCl

- Isolation of Genomic DNA, Blotting, Hybridization

- Speed hyb buffer (7% SDS, 10% Polyethyleneglycol 6000, 1.5 SSPE)
- Tail lysis buffer (10 mM Tris,pH 8, 100 mM EDTA, 1% SDS)
- DNA Isolation Kit (Applichem)
- low TE buffer
- Restriction endonuclease EcoRI (MBI)
- 1kb ladder (Invitrogen)
- 3MM Filter paper (Whatman)
- Nylon membrane (Hybond XL, GE Health Care)
- Multi Prime labeling Kit (GE Health Care)
- 32P-labeled nucleotide (Perkin Elmer)
- TE (10 mM Tris, pH 8, 1 mM EDTA)
- G50 spin column (Roche Diagnostics)

- 2xSSC (20xSSC 3M NaCl, 0,3 M Na₃Citratx2H₂O, 0.5% SDS)

- Staining

- Water-free mounting medium (Eukitt, O. Kindler GmbH & Co)
- Mayer's hematoxylin (Merck #9249)
- Cresyl fast violet solution (0,5 g cresyl fast violet in 100 ml 0,1 M sodium acetate, pH 3.5)
- Weigert's iron haematoxylin (Croma)
- Kluever staining solution [0,1 g Luxol Fast Blue MBSN (Fa. Serva, Best. Nr. 28106, 100 ml 96% ethanol, 0,5 ml 10% aqueous acetic acid)
- Schiff's reagent (Merck #9033)
- Citrate Buffer (4,2028g citric acid monohydrate ad 2000ml a. dest., p.H. 6,0)
- rabbit anti-cow GFAP (Dako Z0334, Glostrup, Denmark)
- vectastain-streptavidin peroxidase Kit (Vector laboratories inc.)
- DAB peroxidase substrate solution (1 ml stock in 9 ml TBS and 60 µl 30% hydrogen peroxide) (Sigma D8001)

Other:

- Embedding cassettes - Tissue-Tek, Sakura, Mega-Cassetten, USA
- Coated glass microscopic slides - HistoBond Adhäsions-Objektträger, Marienfeld GmbH & Co. KG, Landa-Königshofen)
- Steel-blade microtome (MICROM GmbH, Type HM 400 R, Ser. Nr. 10951, Walldorf)

3. METHODS

3.1 Animal Breeding

Mice used in this study were bred at the animal care facility of the Zentrum für Molekulare Neurobiologie (ZNMH), under standard conditions (21°C; relative air moisture 50%; 12 hours light-dark cycle).

$ERR\gamma^{-/-}$ mice were generated by homologous recombination in R1 ES cells by Uwe Borgmeyer. Three targeted ES cell clones (ERR-14, ERR-33, ERR-80) were used to generate chimeric mice by injection of positive ES cells into mouse blastozysts. Male chimeric mice were bred to C57Bl females to generate the F1 generation. Heterozygous F1 mice were subsequently mated to obtain homozygous knock out mice. Because homozygous $ERR\gamma^{-/-}$ mice did not produce offspring, the lines were maintained by mating heterozygous mice to C57Bl wild type mice. Homozygous mice were generated by mating of heterozygous mice, resulting in knock out (ko or $ERR\gamma^{-/-}$), heterozygous (he or $ERR\gamma^{+/-}$), and wild type (wt or $ERR\gamma^{+/+}$) mice in the same litter.

For the purposes of this study both male and female mice were used with ages varying from embryonic day 16 (E16) to adult. The wildtype and heterozygous animals were fed on a standard diet, whereas the knock out animals were fed with soft pellets starting at postnatal day 15. Also, knock out animals that lost weight were hand raised up to P30. The three independently generated knock out mouse lines were phenotypically undistinguishable.

All experimental procedures were approved by the local animal care committee and were in accordance with the guidelines instituted by the German laws for animal experiments.

3.2 Histology

3.2.1 Tissue preparation

Preparation of embryonic tissues

For the removal of prenatal tissues the heterozygous mother was anesthetized with Ketamin/Rompun. The mouse was placed on its back, the lower abdominal area was sagittally sectioned along the course of the linea alba, opening both the layers of the pelt. The uterus was removed and the indirectly anesthetized embryos were retrieved one by one, beginning from the distal one. After washes in PBS to remove the blood, embryos were individually fixated in 4% buffered paraformaldehyd at 4°C over night. For genotyping the tips of the embryos tails were cut off and stored at in the cold until DNA preparation.

3.2.2 Perfusion of postnatal animals

The animals were anesthetized with the same technique and dose as described above. A longitudinal incision along the medial line was performed through the pelt of the abdominal area of the rodent. The diaphragm was then transected under the xiphoid process offering access to the thoracic cavity, which was further opened by the removal of the anterior thoracic wall. With the help of tweezers the heart was kept stable as the right atrium and the jugular veins were incised resulting in terminal bleeding, while a needle was inserted into the left ventricle. It was then possible to perfuse the rodents intracardially with 4% PFA in 0,1M PBS at room temperature at a pressure of approximately 75(mm) Hg.

After the perfusion, the skin over the cranial vault was removed, the later was partially opened and the entire animal was immersed for 2 hours in 4% buffered PFA-solution in order to complete fixation of the body tissues.

After the immersion fixation the following organs were removed: brain, eyes, spleen, kidneys, and the testicles from the male specimens. From the adult animals liver, stomach and lungs were furthermore collected. Esophagus, heart, lymph nodes, spinal

cord, and ovaries of female specimens were removed only from a limited number of experimental mice.

The brain removal was completed as follows; A horizontal cut was performed lower than the level of the medulla oblongata, through the cranium and the spinal cord with a subsequent incision on the course of the sagittal suture from a rostral to a caudal direction. Small coronary incisions aside the latter were then completed and with the help of a pair of tweezers the entire skull was removed in pieces. The brain was then carefully removed with the blunt end of a scalpel, after separating it from the attached cranial nerves and the remaining arachnoid. Due to the small sizes of the prenatal and the younger postnatal mice up to day 3, a stereoscopic magnifying lens was used in order to assist the procedure of the tissue retrieval.

All organs, with the exception of the testicles (s. Semi-thin sections) were then placed in embedding cassettes, where they were fixed for another 24 hours in 4% PFA-solution. Before this procedure brain, kidneys and stomach were treated as described below.

Using a razorblade the brain was sagittally divided along the longitudinal fissure. Both parts were then placed into one embedding cassette.

Every single pair of kidneys was dissected with two cuts. One longitudinal section of one kidney and a transverse section of the other one. The four tissue parts were then combined into two embedding cassettes, each one containing one part of each kidney. The stomach was cut using a surgical scissors, along the major and minor curvature in two parts.

On the next day all the tissues were transferred for another 24 hours in 0,1 M SPB at 4°C.

3.2.3 Sectioning

The cassettes were dehydrated by increasing concentration of 2-Propanol (50%, 70%, 90%, absolute alcohol) followed by embedding into hot molten paraffin wax.

Using a steel-blade microtome, 3 µm for pre- and postnatal up to P3 brain tissue and 5 µm (for all other tissues) thick sections were prepared. The sections were then placed floating on a 40°C warm water bath to remove wrinkles. They were picked up on a coated glass microscopic slide and placed into a drying chamber at 37°C overnight. Before used in the different staining and immunohistochemical protocols the slides were deparaffinised and rehydrated in descending graded ethanol solutions

3.3 Data Analysis

3.3.1 Genotyping

All mice used in this study were genotyped using the Southern blot technique.

3.3.2 Isolation of genomic DNA

Tail tips were lysed overnight at 55°C in 0.5 ml tail lysis buffer. The DNA was isolated from the lysate using the DNA Isolation Kit according to the manufacturer's instructions. In brief, 0.5 ml of the isolation reagent was added to the tail lysates, mixed by inversion and incubated at room temperature for five minutes. 1 ml of 100% Ethanol was added, the solution was mixed by inversion, incubated for three minutes at room temperature and then centrifuged at 9000 rpm (Heraeus microfuge) for 15 min. The supernatant was pipetted and the pellet was washed twice with 96% Ethanol. After drying the DNA was dissolved in 100 µl of low TE buffer at 37° C for at least two hours.

3.3.3 Restriction digests and gel electrophoresis

20 µl of the genomic DNA was digested in a total volume of 50 µl using 20 units restriction endonuclease EcoRI at 37° C overnight. The reactions were stopped by addition of 5 µl of loading buffer and then loaded on a 0.8% agarose gel in TAE buffer containing ethidium bromid. The gel was run in TAE buffer at 120 V for up to 8 hours. For documentation gels were placed on an UV-light and photographed placing a ruler adjacent to the gel. The 1kb ladder was used as a size marker.

3.3.4 Blotting

The gel was placed in 0.25 M HCl, rinsed with deionized water and incubated in 0.4 M NaOH for 15 minutes. Then, it was placed on a 3MM Filter paper covering a filter bridge extending into 0.4 M NaOH . The areas of the filter paper not covered by the gel were sealed using saran wrap and the nylon membrane pre-equilibrated in 0.4 M NaOH for at least 5 minutes was placed onto the gel. The slots were marked with pencil. Two additional 3 MM papers were put on top of the membrane and a stack of paper towels was added onto which a glass plate and a weight, depending on the size of the gel to be

transferred was added. When the paper towels were soaked with the transfer solution they were removed and the nylon membrane was placed on top of 2 x SSC solution for approximately 5 minutes before it was baked at 80° C for two hours.

3.3.5 Preparation of the radioactively labeled probe by random priming

For radioactive labeling the Multi Prime Labeling Kit was used according to the manufacturer's instructions. In brief, 25 ng of the ERR γ specific DNA-fragment, supplied by PD Dr. Uwe Borgmeyer, were denatured in the presence of 5 μ l random primer for 5 minutes at 96° C, chilled on ice. Reaction buffer (5 μ l), three non-labeled nucleotides (4 μ l each), the 32P-labeled nucleotide and 2 μ l Klenow enzyme were added in a total volume of 50 μ l. The reaction was incubated for 15 minutes at 37° C, stopped by addition of 50 μ l TE buffer and loaded on a G50 spin column prepared according to the manufacturer's instructions, and centrifuged for 5 minutes at 1500 x g. The eluate was transferred to an Eppendorf tube and 1 μ l fluid was removed for scintillation counting. Prior to hybridization the probe was denatured for 5 minutes at 96° C.

3.3.6 Hybridization

The nylon membrane was placed in a roller incubator tube and depending on the size of the membrane 5 – 20 ml of speed hyb buffer containing 100 μ g/ml of denatured herring sperm DNA was added and incubated at 65° C for at least 30 minutes. For hybridization fresh, pre-warmed speed hyb buffer containing 2.5 x 10⁵ cpm of the radioactively labeled probe were added and the incubation continued over night.

For washes the hybridization solution was discarded and the roller tube was filled with 2 x SSC (wash 1) pre-warmed to 65° C. After shaking of the roller tube this buffer was discarded and the tube was filled to the half with fresh pre-warmed wash 1 and incubated rolling for 20 minutes. This wash step was repeated twice. Wash 1 was then replaced by 0.1 x SSC, 0.1% SDS for at least 10 minutes. After washing the membrane was exposed to a phosphoimagerplate for 1–3 hours.

3.4 Staining procedures

3.4.1 Hematoxylin-Eosin Staining

The rehydrated slides were first placed in Mayer's hematoxylin for 3 minutes, followed by distilled and tap water for 2 and 5 minutes, respectively. Then they were stained in 0,5% Eosin for 3 minutes, followed by distilled water for 30 seconds, 70% ethanol for 15 seconds, 96% ethanol for 2 x 30 seconds, absolute ethanol for 2 x 5 minutes, and xylene for 3 x 5 minutes.

3.4.2 Mounting

After a swab of the slide surface one drop of water-free mounting medium was added . A square cover slip was then carefully placed over the specimens. In order to avoid air bubbles pressure was applied over the cover slip with a filter paper. The slides were then kept overnight flat and undisturbed in a dust free area.

3.4.3 Nissl-Staining with Cresyl-violet

The deparaffinised and rehydrated tissues were stained for 9 ½ minutes in a Cresyl fast violet solution. Subsequently, the slides were rinsed twice with buffer solution (0,1 M sodium acetate, pH 3.5) and differentiated in 96% ethanol, acidified by addition of 3 drops of acetic acid. The slides were dehydrated in 100% ethanol for a few seconds and mounted as described above.

3.4.4 Masson-Goldner's trichrome staining

The tissues were deparaffinated and partially rehydrated as described above. They were placed in a solution of Weigert's iron haematoxylin for 3 - 8 minutes, then washed shortly and differentiated in hydrochloric-alcohol solution for 10 - 30 seconds. To stop the differentiation process the slides were washed with running tap water. The slides were washed shortly in distilled water and then submerged into 1% Ponceau-acetic acid solution for 5 - 10 minutes, differentiated in 1% phosphomolybdic acid for approximately 10 minutes. They were washed in 1% acetic acid for 1 minute and counterstained in a solution of light green for approximately 3 minutes followed by two

washes with 1% acetic acid for 30 seconds and 5 minutes, respectively and then dehydrated and mounted as described above.

3.4.5 Kluever-Barrera staining

The rehydration process of the slides was stopped reaching the 96% ethyl alcohol, in which they were kept for 10 minutes. Then they were submerged into the Kluever staining solution for 2 hours at 56° C. The slides were washed in 96% ethyl alcohol and distilled water. Hereafter, they were differentiated for 20 seconds in 0,05% aqueous lithium carbonate solution (Fa. Merck, Best. Nr. 5671,) followed by 70% alcohol under microscopic control. For differentiation the slides were washed in distilled water. In case it was necessary to repeat the differentiation process this was done by re-submerging the slides into the 0,05% aqueous lithium carbonate solution. The slides were counterstained with cresyl-violet ending up in xylene and mounted as already described.

3.4.6 Periodic Acid Schiff Reaction (PAS)

After rehydration the slides were submerged in period acid for approximately 20 minutes, rinsed in tap water followed by distilled water and then placed in Schiff's reagent (Merck #9033) for 15 minutes, followed by washes with distilled water and tap water for about 10 minutes. They were counterstained with Mayer's haematoxylin for 2 minutes and washed with tap water until the haematoxylin was blued. Finally, the slides were dehydrated with ethanol, cleared with xylene and mounted as already described above.

3.5 Immunohistological Stainings

3.5.1 Anti-GFAP

For the specific demonstration of the astrocytes, the rabbit anti-cow GFAP (Dako Z0334, Glostrup, Denmark) was used in a dilution of 1:800 as the primary antibody. After the rehydration of the slides the slides were placed in a plastic cuvette containing citrate buffer into the microwave oven at 1000 Watt until the solution reached its boiling temperature and then they were processed for 5 cycles each lasting 2 minutes at 500 Watt. The slides were left to cool to room temperature. For the inactivation of the endogenous peroxidase activity the slides were incubated in 3% H₂O₂ in Methanol for 20 minutes. Then they were washed 2 x 5 minutes in TBS (Trizma base, minimum, T 1503, SIGMA-ALDRICH, Steinheim) followed by the incubation of the sections in swine serum diluted in antibody diluent with background reducing components (DAKO S3022, Glostrup, Denmark) 1:10 for 30 minutes to block non-specific binding of immunoglobulin. Finally, the sections were incubated overnight at 4° C with the primary antibody diluted 1:800. The following day the slides were rinsed 2 x 5 minutes with TBS and incubated for 30 minutes at room temperature with the biotinylated Pig Anti-Rabbit secondary antibody diluted 1:200. After the slides were rinsed 2 x 5 minutes with TBS, they were incubated for another 30 minutes at room temperature with the vectastain-streptavidin peroxidase Kit. The slides were rinsed 2 x 5 minutes in TBS and then incubated in DAB peroxidase substrate solution for 10 minutes. They were rinsed in running water for 5 minutes and dehydrated in alcohol solutions of ascending concentrations, ending up in xylene and mounted as already described above.

3.5.2 Anti-Tyrosine Hydroxylase (Anti-TH)

In order to assess the tyrosine hydroxylase positive neurons in all three genotypes, both sagittal and coronal sections were stained. The hemispheres of two adult triplets were used for the sagittal sections, whereas for the coronal sections the hemispheres of one adult triplet and one diplet (ERR $\gamma^{+/+}$ and ERR $\gamma^{-/-}$) were examined. For the localization of the mesencephalic substantia nigra both on the sagittal and the coronal sections the “Atlas of the Mouse Brain and Spinal Cord” (34) was used.

For both views, serial sections -sagittal or coronal- were cut (5 μm), and Nissl stained in order to determine the exact location of the substantia nigra, after which the adjacent sections were processed for TH immunoreactivity using a polyclonal rabbit anti-tyrosine hydroxylase antibody. The slides were prepared by microwave irradiation (see 3.5.1). Following the inactivation of the endogenous peroxidase activity and the blockage of non-specific binding of immunoglobulins, the slides were incubated overnight at 4°C with the primary antibody in a dilution of 1:500. The next day a biotinylated Swine Anti-Rabbit in a dilution of 1:200 was applied. After the incubation with the Vectastain-Pox complex for 30 minutes and the DAB peroxidase substrate solution incubation for approximately 10 minutes the slides were ready for dehydration and mounting.

3.6 Morphometric Analysis

Paraffine blocks of the left or right brain hemispheres, six of each of the 3 different phenotypes were serially sagittally sectioned. Every tenth serial section was then Nissl-stained and analyzed using the Axiophot 2 microscope. In order to assure that sections of the same mediosagittal level of the different brains were subjected to morphometric analysis every fifth serial section was additionally stained with Nissl stain. The “Atlas of the Mouse Brain and Spinal Cord” (34) was used as reference to identify the brain regions.

After the selection of the appropriate sagittal brain sections images were then taken using an Axiophot 2 microscope and the Axiovision (Zeiss) program. Next to each section a millimeter ruler was placed serving as a measuring benchmark. Images were captured while the focusing setting of the camera was kept constant through out the capturing.

All photographs suitable for morphometric analysis were simultaneously opened, and measured one by one for each region. For the first measured region 10 consecutive serial repetitions were performed in order to assess the statistical variations of the results. For each of the other regions three consecutive serial repetitions were sufficient to establish a statistical significant result. During the measurements the genotypes of the analyzed sections were blinded and not known. With the help of a millimeter ruler, which was photographed using the same settings as used to take the pictures of the brain the correlation between pixels and millimeters was established.

Five out of six triplets were artifact-free and were finally used for the purposes of this analysis. Apart from total brain surface size counts, the following regions were also measured:

1. telencephalon,
 - i. telencephalic cortex,
 - ii. hippocampus,
 - iii. telencephalic white matter
2. diencephalon
3. mesencephalon
 - i. mesencephalic tectum

- ii. mesencephalic tegmentum
- 4. cerebellum
 - i. cerebellar white matter
 - ii. cerebellar cortex
- 5. pons

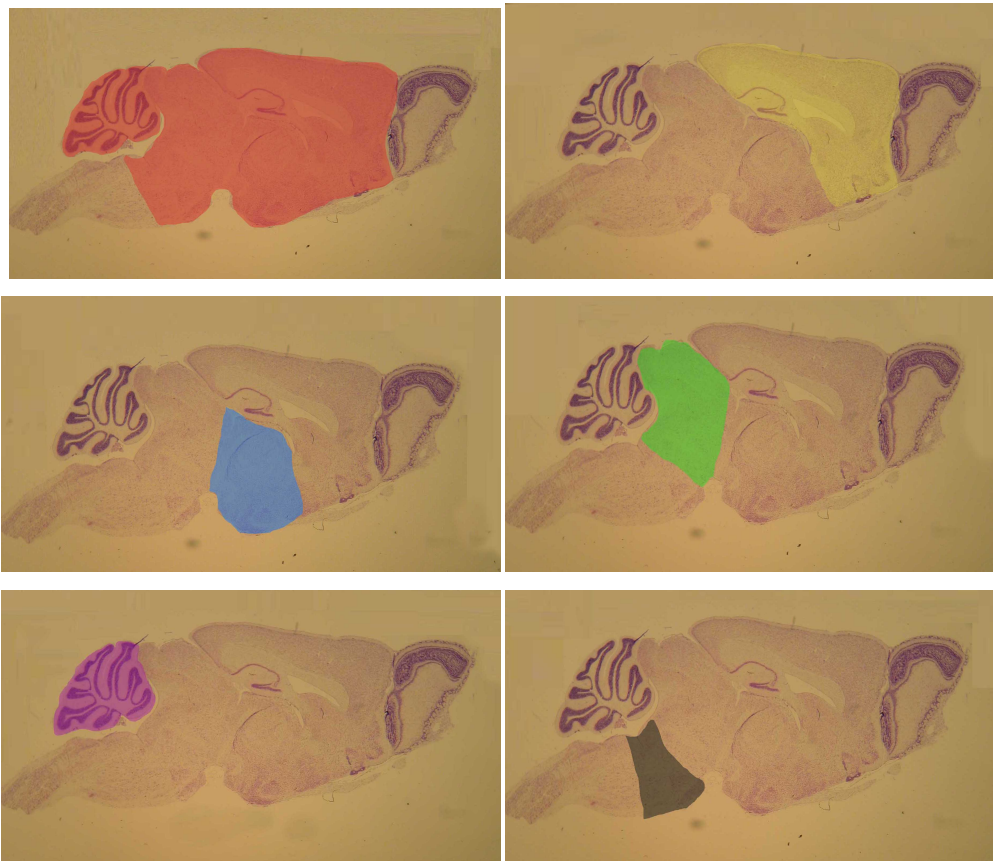


Fig. 3 Brain areas measured and compared between the three genotypes. The total brain area (red), the telencephalic area (yellow), the diencephalon (blue), the mesencephalon (green), the cerebellum (purple) and the pons (grey) were analyzed.

The spatial definition of each area was accomplished with the help of the “Atlas of the Mouse Brain and Spinal Cord” (34).

For the total-brain-surface size the perimeter between two frontiers was measured. The dorsal brain frontier was established with a transverse line connecting the most caudal part of the cerebellum with the medulla oblongata, excluding the spinal tract nucleus. The cerebellar surface was estimated following the foliate pattern where possible. The olfactory bulb was not included in any of these analyses (Fig. 3).

The measurement of the telencephalic surface included the telencephalic cortex and white matter and was separated from the diencephalon with a transverse line rostral to the thalamic nuclei, including the anterior commissure of the forebrain (Fig. 3).

The telencephalic cortex, the hippocampus and the telencephalic white matter are well-defined areas (34); therefore the description of their borders will not be given in further detail.

The diencephalon was defined and measured as the extending area behind the anterior commissure of the forebrain, caudally separated by the mesencephalon with a diagonal line excluding the accessory nucleus of the oculomotor nerve. The hypothalamic structures were included in the diencephalic measurements.

The rostral border of the mesencephalic area was defined through the telencephalic occipital cortex and the dorsal diencephalic area. The caudal frontier was defined with a diagonal line including the dorsal raphe nucleus but excluding the tegmental reticular nucleus of the pons (Fig. 3).

The size of the cerebellum was measured so, following the foliar pattern when possible. The size of the cerebellar white matter was then determined and subtracted from the value of the total cerebellar size. Cells of the deep cerebellar nuclei were additionally measured and added to the estimated values of the cerebellar cortex (Fig. 3).

For the assessment of the pons the rostral borders were set as the dorsal side of the mesencephalic area and the dorsal borders were defined with a transverse line between the dorsal and the ventral part of the brainstem including the nucleus centralis caudalis pontis (Fig. 3).

In order to assess the size differences of each area of the two genotypes (WT and KO) neutralizing their absolute brain size differences, the acquired values were normalized to the total brain size of each genotype, as demonstrated:

$$\text{Normalized Value For Genotype} = \frac{\text{Region Of Genotype}}{\text{Total Brain Size Of Genotype}} \times 100\%$$

For example, the telencephalic values of one littermate pair of a WT and a KO resulted as follows:

$$\text{Normalized Telencephalic Value WT} = \frac{\text{Telencephalic Region Of WT}}{\text{Total Brain Size Of WT}} \times 100\% = \frac{3.29\text{mm}^2}{9.22\text{mm}^2} \times 100\% = 35.7\%$$

$$\text{Normalized Telencephalic Value WT} = \frac{\text{Telencephalic Region Of KO}}{\text{Total Brain Size Of KO}} \times 100\% = \frac{2.52\text{mm}^2}{6.79\text{mm}^2} \times 100\% = 37.1\%$$

A statistical analysis was performed using the SPSS program and applying the t-test for unpaired probes.

4. RESULTS

4.1 Determination of the genotypes of the ERR γ used in this study

4.1.1 Southern Blotting

Because the ERR γ ^{-/-} mouse line had to be propagated by heterozygous mating genotyping was necessary to distinguish between the different phenotypes resulting from such mating.

To determine the phenotypes of the experimental animals genomic DNA was isolated from mouse-tail biopsies and after a restriction digest with EcoR1 was separated by gel electrophoresis and subsequently analyzed by Southern blotting using a 3' located probe outside the homology region. As demonstrated in figure 4 heterozygous mice displayed an upper wild type signal at 15 kb and a lower signal at 11 kb, while in wildtype offspring only the upper band appeared and in the knock out mice only the lower band.

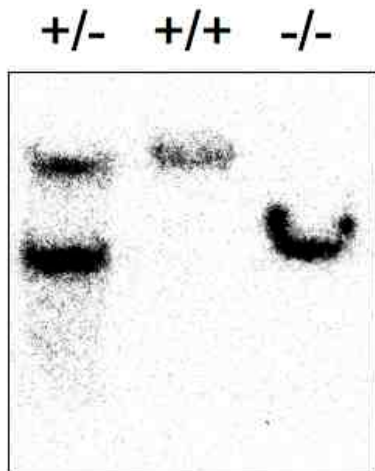


Fig. 4 Southern Blot for the genotypic determination of the ERR γ mice. EcoR1 digested DNA of the genotypes indicated was separated on a 0.8% agarose gel and subjected to Southern blotting. For detection a ³²P-dATP labeled 3' of the homology region was used and a Fujix BAS Reader for the visualization of the signals. ERR γ ^{+/-} (+/-, left) displayed an upper wild type signal at 15 kb and a lower signal at 11 kb, while in ERR γ ^{+/+} (+/+, middle) offspring only the upper band appeared and in the ERR γ ^{-/-} mice (-/-, right) only the lower band

4.1.2 General Observations

A total number of 154 mice of different ages were used for the purposes of this study. To determine whether the transgenic animals showed an increased lethality, the distribution of genotypes at various stages of development was determined. The weight and vertex-breech length were also measured in order to reveal delayed growth and development.

Following parameters were evaluated and demonstrated:

4.1.3 Genotypic Distribution

To determine whether the lack of $ERR\gamma$ resulted in an increased lethality during embryonic or early postnatal development, the distribution of genotypes in fetuses and in surviving mice was analyzed. Because heterozygous matings were used, statistically 25 % of the offspring should be $ERR\gamma^{+/+}$ (WT), 50 % $ERR\gamma^{+/-}$ (HE) and 25 % knock out ($ERR\gamma^{-/-}$) animals.

At embryonic (e) day 16, a total of 21 fetuses was collected, biopsied and intracardially perfused. Genotyping revealed that 10 mice (47.6%) were $ERR\gamma^{+/-}$, 8 mice (38.1%) were $ERR\gamma^{+/+}$ and 3 mice (14.3 %) were $ERR\gamma^{-/-}$.

At E18, out of a total of 16 fetuses, 10 mice (62.5%) were $ERR\gamma^{+/-}$, followed by $ERR\gamma^{+/+}$ and $ERR\gamma^{-/-}$ both represented by 3 mice each (18.75%).

At postnatal day (P) 1, out of a number of 32 biopsied and perfused mice, 24 mice (75%) were $ERR\gamma^{+/-}$, followed by 5 mice (15.6 %) $ERR\gamma^{+/+}$ and 3 mice (9.4%) $ERR\gamma^{-/-}$.

Finally, at P3, the biopsy results showed that out of 26 examined mice, 13 (50%) of them were $ERR\gamma^{+/-}$, 11 (42.3%) were $ERR\gamma^{+/+}$ and 2 (7.7%) $ERR\gamma^{-/-}$.

These results demonstrate that $ERR\gamma^{-/-}$ animals were underrepresented in the postnatal phase pointing to an increased lethality of the phenotype.

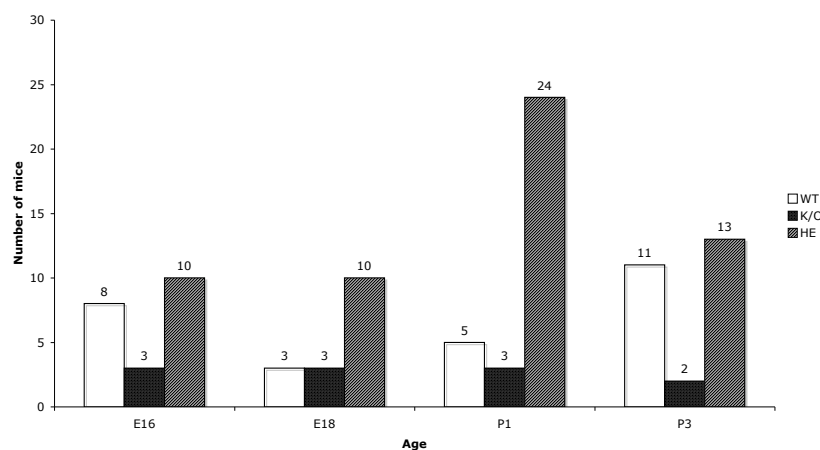


Fig. 5 Absolute values of the genotypic distribution for the $ERR\gamma^{+/+}$, $ERR\gamma^{-/-}$ and $ERR\gamma^{+/-}$ mice at four developmental stages (E16, E18, P1 and P3), revealing postnatal underrepresentation of the $ERR\gamma^{-/-}$ mice beginning from P1.

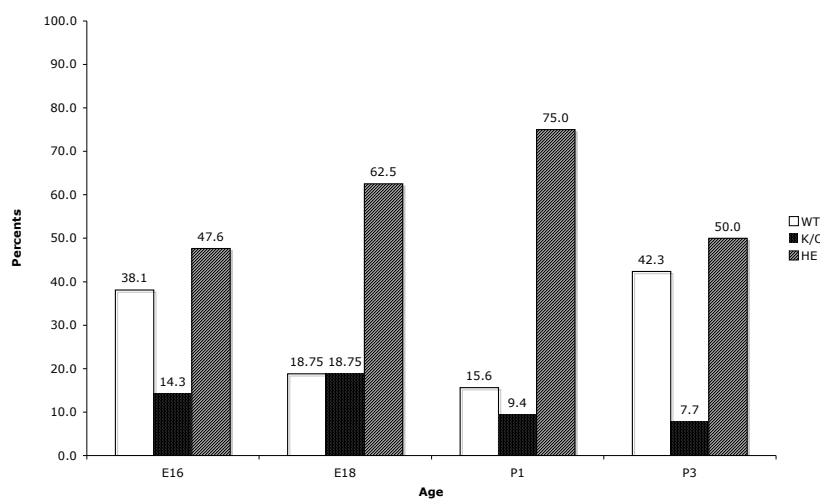


Fig. 6 Genotypic distribution for the $ERR\gamma^{+/+}$, $ERR\gamma^{-/-}$ and $ERR\gamma^{+/-}$ mice at four developmental stages (e16, e18, p1 and p3) given in percentage, showing postnatal underrepresentation of the $ERR\gamma^{-/-}$ mice beginning from P1.

4.2 Demonstration of Adult weight differences between the $ERR\gamma^{+/+}$ and the $ERR\gamma^{-/-}$ animals

The weights of eight adult mice triplets were measured. At figure 7 a scatter diagram of the weight of all the adult mice is shown.

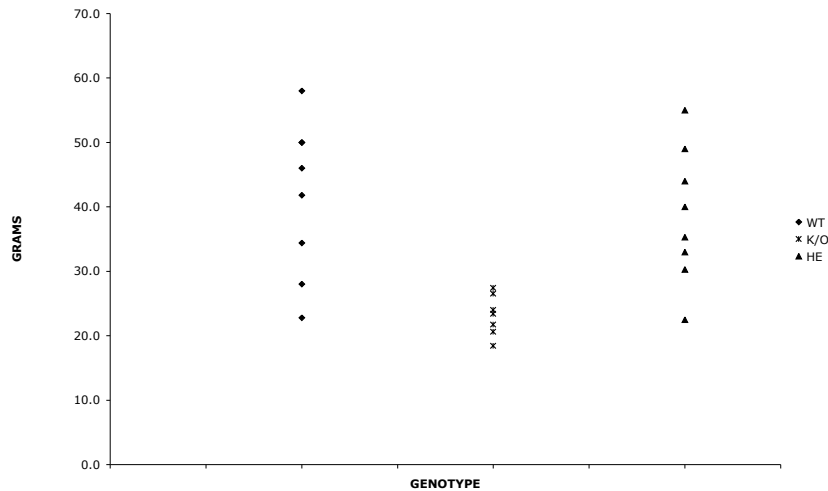


Fig. 7 Scatter diagram of the numeric values of the - eight pro genotype- adult mice body weights, indicating marked absolute body weight reduction of the $ERR\gamma^{-/-}$ mice. As shown at figure 8, the average weight of the $ERR\gamma^{+/+}$ mice was 41.4 g (standard error of the mean (SEM) 4.3), that of the $ERR\gamma^{-/-}$ 24.3 (SEM 1.5) and of the HE 38.6 g (SEM 3.7). Normalized to the $ERR\gamma^{+/+}$ adult mice weight (100%), the $ERR\gamma^{-/-}$ mice weighted 58.6% while the $ERR\gamma^{+/-}$ 93.4% (fig. 9).

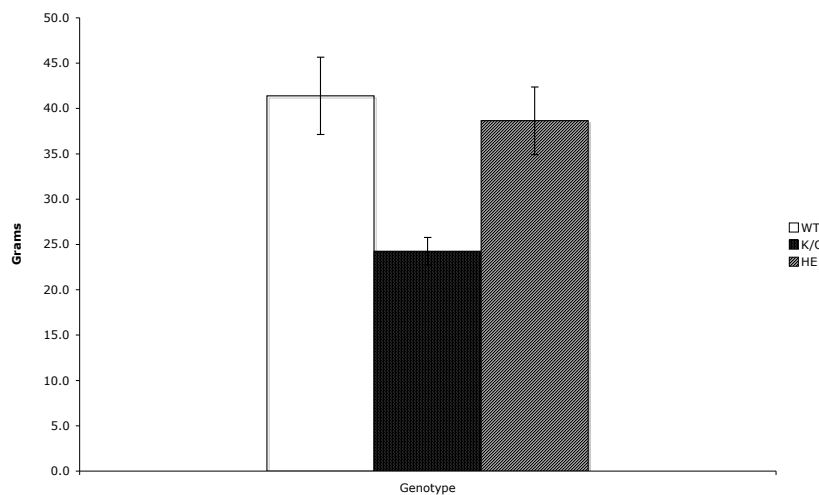


Fig. 8 Average adult body weight values of the three genotypes with SEM (n of each

genotype =8), revealing the marked weight reduction of the $ERR\gamma^{-/-}$ mice of 17.1 g.

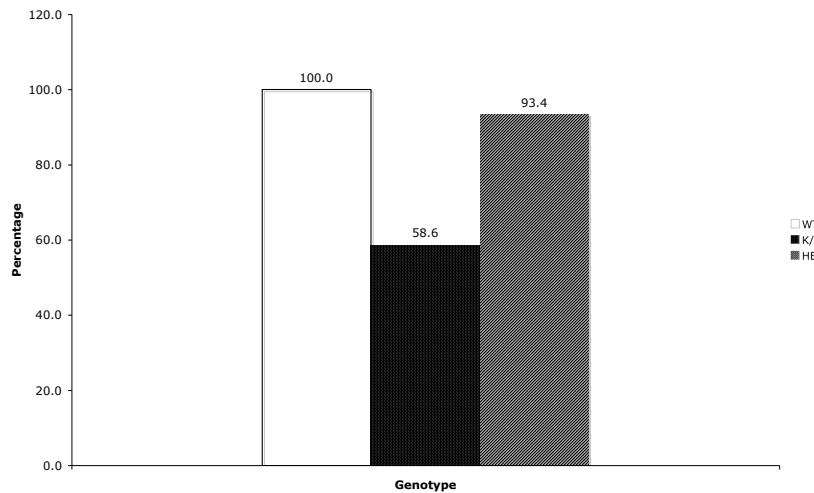


Fig. 9 Average adult body weight values of the three genotypes normalized to the $ERR\gamma^{+/+}$, showing a the 41.4% body weight reduction of the $ERR\gamma^{-/-}$ mice compared to their wildtype littermates.

At figure 10 the evaluation of each separate $ERR\gamma^{+/+}$ - $ERR\gamma^{-/-}$ littermate pair is demonstrated.. The values of the $ERR\gamma^{-/-}$ mice weight varied between 80.7% and 45.7% of their $ERR\gamma^{+/+}$ littermate's weight.

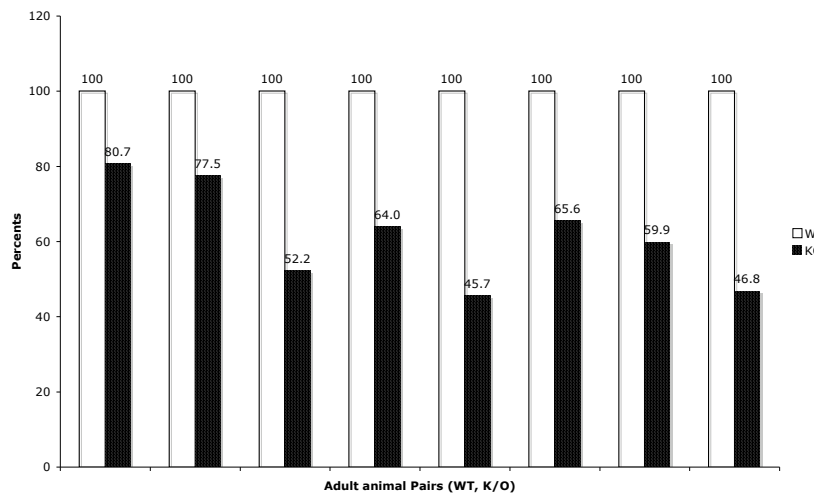


Fig. 10 Evaluation of the body weight of the $ERR\gamma^{+/+}$ - $ERR\gamma^{-/-}$ littermate-pairs. Depicted are the $ERR\gamma^{+/+}$ body weight values (100%) and the $ERR\gamma^{-/-}$ values normalized to the ones of their $ERR\gamma^{+/+}$ littermate, revealing a body weight underrepresentation of all $ERR\gamma^{-/-}$ mice compared to their $ERR\gamma^{+/+}$ littermates.

These results show that the $ERR\gamma^{-/-}$ animals were characterized by a reduction of body weight in the adult stage.

4.3 The determination of the beginning of the $ERR\gamma^{-/-}$ weight reduction compared to the $ERR\gamma^{+/+}$

In order to analyze if the weight differences observed between adult $ERR\gamma^{+/+}$ and $ERR\gamma^{-/-}$ animals were established before or after weaning, the weight was determined at different stages of development.

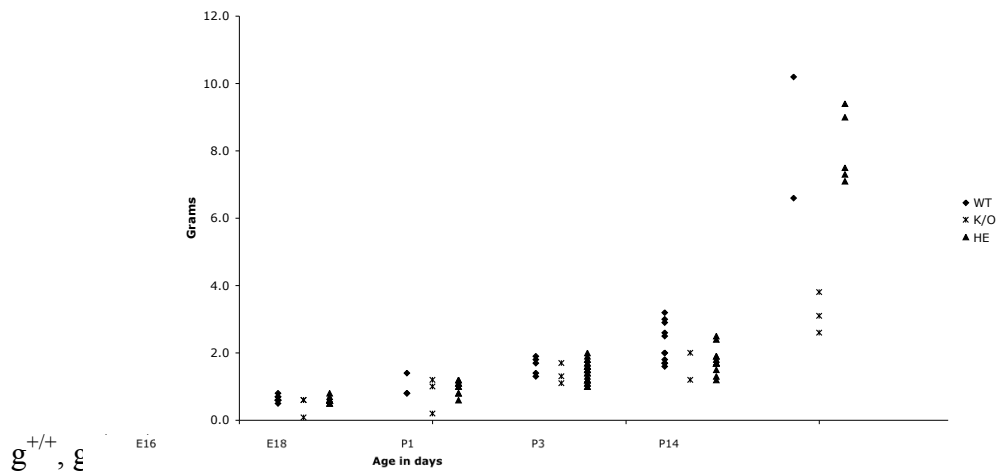


Fig. 11 Scatter diagram of body weight values of all the mice assessed at five different developmental stages (E16, E18, P1, P3 and P14), showing a body weight reduction of the knockout mice onwards from P1.

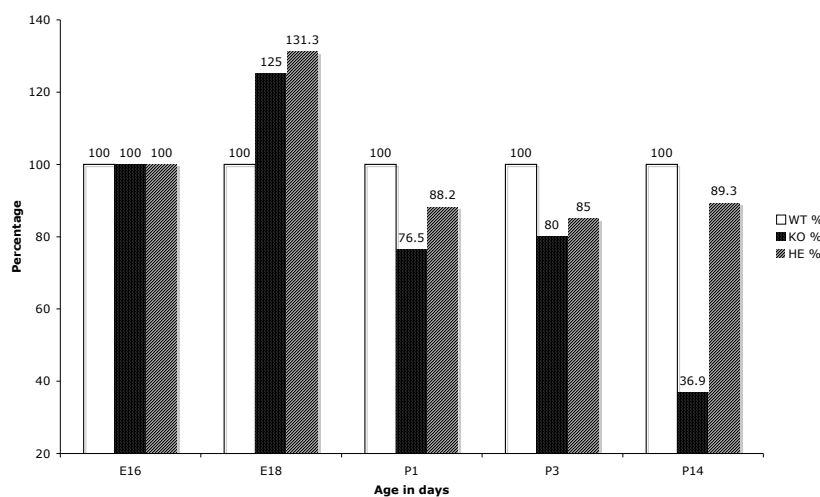


Fig. 12 Median body weight values of the assessed mice of all three genotypes normalized to the $ERR\gamma^{+/+}$ mice values showing a considerable weight reduction of the $ERR\gamma^{-/-}$ mice beginning from P1.

No prenatal weight reduction of the $ERR\gamma^{-/-}$ mice compared to the $ERR\gamma^{+/+}$ could be detected during development (see figures 11 and 12). From P1 onwards the mice had a 23.5% body weight reduction, at P3 a reduction 20% and at P14 63.1%. This observation is indicative for a postnatal factor accounting for this progressive body weight decrease.

4.4 Demonstration of adult vertex-breech-length differences between the $ERR\gamma^{+/+}$ and the $ERR\gamma^{-/-}$ animals

In order to analyze whether the reduced weight of the adult $ERR\gamma^{-/-}$ mice was correlated to a reduced size the vertex-breech-length was measured (Figure 13).

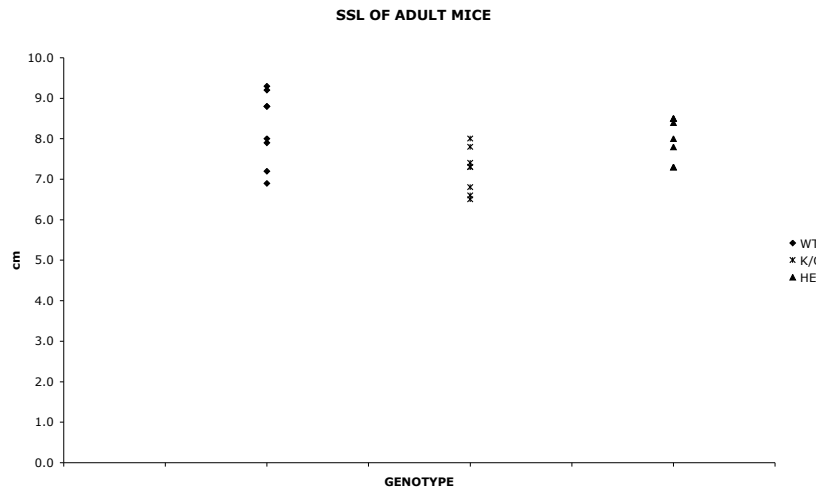


Fig. 13 Scatter diagram of the adult mice vertex-breech-length of the three genotypes (n= 8), showing an overt smaller size of the $ERR\gamma^{-/-}$ mice compared to their $ERR\gamma^{+/+}$ littermates.

As shown at figures 14 and 15 the average vertex-breech length of the $ERR\gamma^{-/-}$ mice was with 7.2 cm (normalized value 87.3%) significantly smaller than the ones of the $ERR\gamma^{+/+}$ (8.3 cm, 100%) and the $ERR\gamma^{+/-}$ (8.0 cm, 97.3%) littermates.

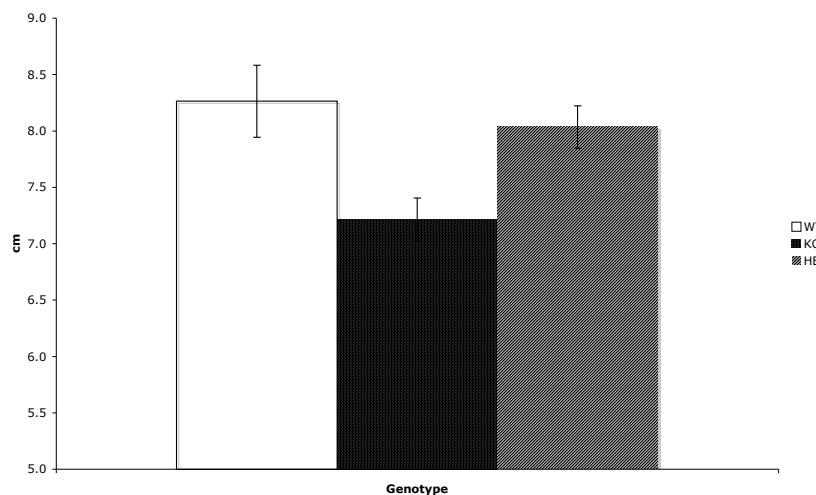


Fig. 14 Average adult vertex-breech-length values of the three genotypes with SEM (n of each genotype =8). $ERR\gamma^{+/+}$ mice 8.3 cm (SEM ± 0.3), $ERR\gamma^{-/-}$ mice 7.2 cm (SEM \pm

0.2) and $ERR\gamma^{-/-}$ mice 8.0 cm (SEM \pm 0.2), indicating the smaller length of the $ERR\gamma^{-/-}$ mutants compared to their littermates.

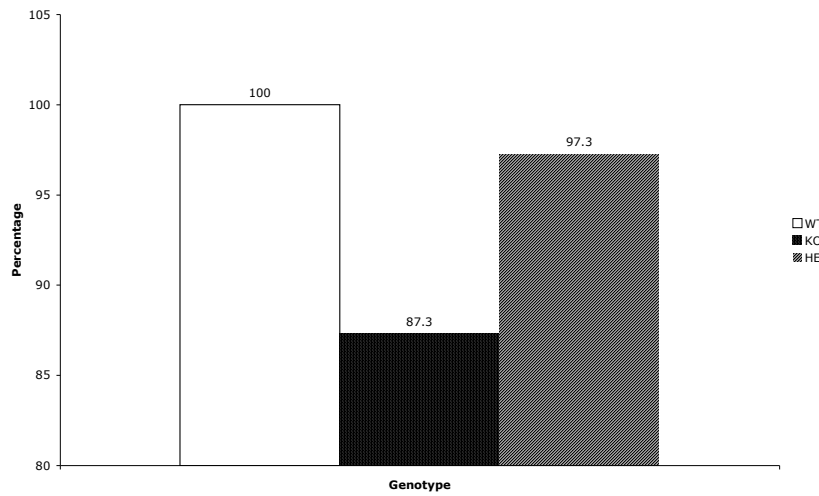


Fig. 15 Average adult vertex-breech-length values of the three genotypes normalized to the $ERR\gamma^{+/+}$, signifying a marked length reduction of the $ERR\gamma^{-/-}$ mice compared to their $ERR\gamma^{+/+}$ littermates ($ERR\gamma^{+/+}$ vertex-breech length 100%, $ERR\gamma^{-/-}$ 87.3 % and $ERR\gamma^{+/-}$ 97.3%).

The evaluation of the vertex-breech-length of each separate $ERR\gamma^{+/+}$ - $ERR\gamma^{-/-}$ pair is shown at figure 16.

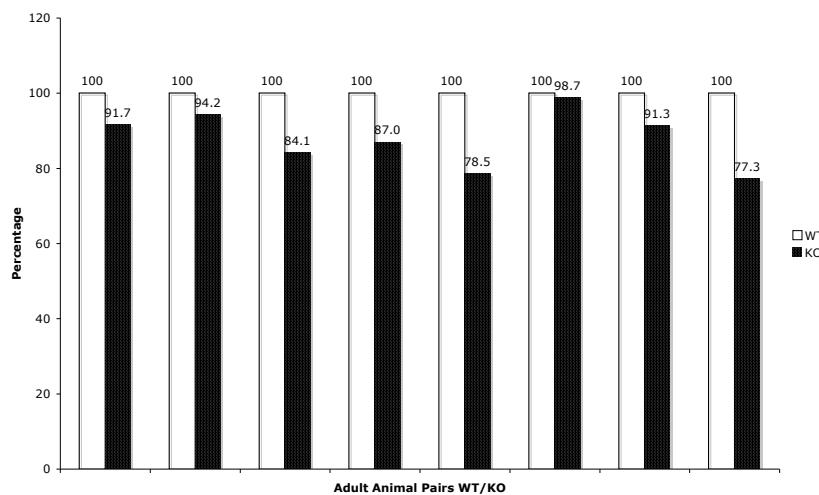


Fig. 16 Evaluation of the vertex-breech-length of the $ERR\gamma^{+/+}$ - $ERR\gamma^{-/-}$ littermate-pairs. $ERR\gamma^{-/-}$ values normalized to the ones of their $ERR\gamma^{+/+}$ littermates, revealing a reduction in size of all $ERR\gamma^{-/-}$ mice compared to their $ERR\gamma^{+/+}$ littermates.

These results show a reduction of the vertex-breech-length of 13 %, which is unlikely to account for the 40 % reduction of body weight described in chapter 4.2.

4.5 $ERR\gamma^{-/-}$ mouse growth delay compared to the $ERR\gamma^{+/+}$ mice.

To examine whether the reduced length observed in the adult mice was already established during development, the vertex-breech length values of the mice during the various developmental stages were calculated and are shown at figure 17.

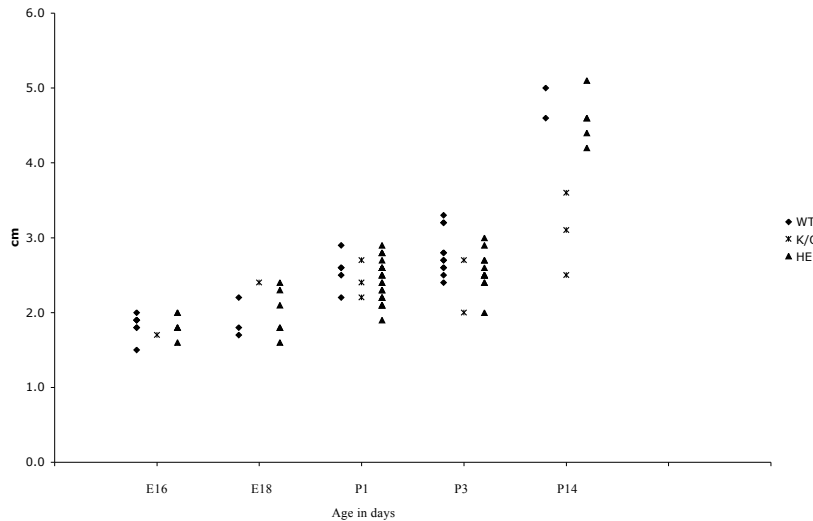


Fig. 17 Scatter diagram of the absolute vertex-breech-length values of all the mice at five developmental stages (E16, E18, P1, P3 and P14), showing a clear growth delay of the $ERR\gamma^{-/-}$ mice postnatally.

Figure 18 shows the median vertex-breech-length values of the $ERR\gamma^{-/-}$ mice at the different developmental stages and figure 19 presents these values normalized to the $ERR\gamma^{+/+}$ mean.

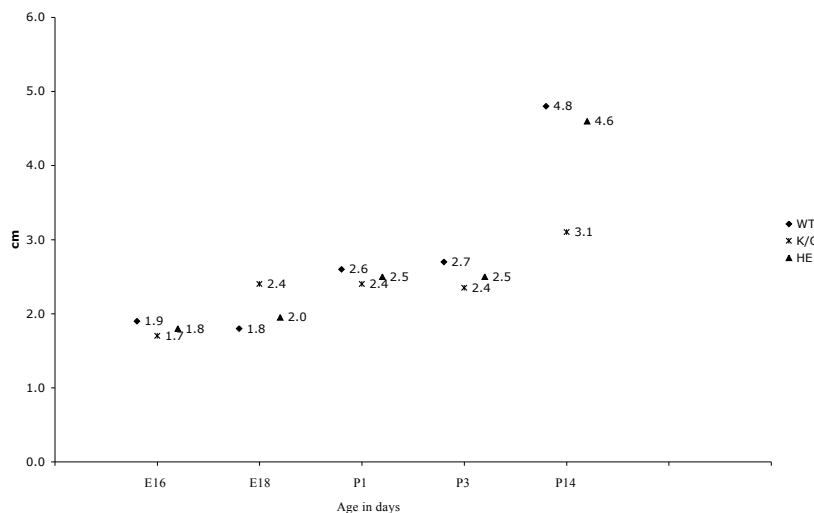


Fig. 18 Median vertex-breech-length of all assessed mice of the three genotypes at five

developmental stages (E16, E18, P1, P3 and P14), showing the relative growth reduction from of the $ERR\gamma^{-/-}$ mice starting from P1.

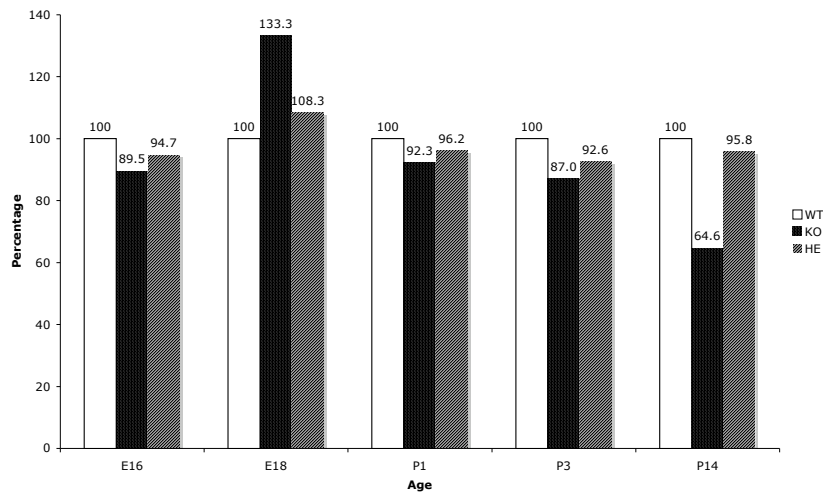


Fig. 19 Median vertex-breech-length values of the assessed mice of all three genotypes normalized to the $ERR\gamma^{+/+}$ mice values with the $ERR\gamma^{-/-}$ mice exhibiting growth delay from p 1.

These results show, that the lack of $ERR\gamma$ expression becomes phenotypically evident only postnatally (median normalized vertex-breech-length values of $ERR\gamma^{-/-}$ to $ERR\gamma^{+/+}$: E16 82.5%, E18 133.3%, P1 92.3%, P3 87%, P14 54.5%).

4.6 Neurological Phenotype

Undisturbed, $ERR\gamma^{-/-}$ mice lied on their abdomen. A posturing kyphosis was frequently observed. They hardly showed any spontaneous activity; rarely did they try to move forward. Their principally hypokinetic gait was characterized by slow, intense, tremorous movements. Involuntary backward-walking (retropulsion) was also seen. When they moved, their forelimbs showed intact motor functions, while the hind limbs regularly demonstrated sustained contractions, resembling dystonic reactions or actions myoclonus, leading to repetitive circling body movements (waltzing). When placed on their back, they tended to outstretch all of their four limbs. When lifted up by the tail and flicked backwards through the air they frequently landed on their back and their righting-reflex, i.e. the ability of coming back onto their feet, required greater effort and a more prolonged time, as compared to control mice. When pressure was gently exerted with the fingertip onto the plantar surface of their paws, the forelimbs displayed moderate resistance. The resistance of the hind limbs varied from very weak to extremely strong, in comparison to the wildtype control animals. When the $ERR\gamma^{-/-}$ mice were lowered and allowed to grip a grid they exhibited a variable but extremely strong grip strength, while the control wildtype mice exhibited a milder response. Under stressful events (e.g. when put in a new environment) permanent tail elevation was observed, resembling a dystonic contraction. The $ERR\gamma^{-/-}$ mice never exhibited signs of aggression or sexual behavior, only seldom and strictly under provocation did they vocalize, whereas fear-responses (eg. to a loud sound) often led to freezing during transfer arousal.

Mainly due to the marked hypokinesia, but also due to the additional the locomotor symptoms, all of our attempts to analyze and record the stepping patterns of the $ERR\gamma^{-/-}$ mice using ink-marks did not lead to any success. Likewise, during our attempts to assess the ability of these animals to walk on a rotating bar (rotarod), all of the $ERR\gamma^{-/-}$ mice, with the exception of one, immediately fell off the bar at the beginning of the rotation. In the case of the exception, the $ERR\gamma^{-/-}$ mouse rotated along with the bar due to the unusually effective grip strength it exhibited.

4.7 Morphology

4.7.1 Gross morphology

While at the gross anatomical level the $ERR\gamma^{+/-}$ mice appeared healthy and had normal life spans, null-mutants could be reliably macroscopically identified at approximately three days post partum based on their posture, their reduced weight ($ERR\gamma^{+/+}$ median weight 2.0 grams, $ERR\gamma^{-/-}$ median weight 1.6 grams) and vertex-breech-length ($ERR\gamma^{+/+}$ median vertex-breech-length 2.7cm, $ERR\gamma^{-/-}$ median vertex-breech-length 2.4 cm) (figs. 20, 21), as well as their neurological phenotype (see chapter 4.6). No other macroscopic alterations were observed.



Fig. 20 Adult duplet, $ERR\gamma^{+/+}$ and $ERR\gamma^{-/-}$ (arrow). The $ERR\gamma^{-/-}$ mouse (arrow) has a reduced body weight (average adult $ERR\gamma^{-/-}$ body weight 58.6% of the average $ERR\gamma^{+/+}$ value) and size (average adult $ERR\gamma^{-/-}$ vertex-breech-length 87.3% of the average $ERR\gamma^{+/+}$ value) and outspread hindlimbs at rest.



Fig. 21 Genotypic littermate triplet of mice at the age of p14. The $ERR\gamma^{-/-}$ mouse can be differentiated from it's littermates by its reduced body weight (at p14 mean $ERR\gamma^{-/-}$ body weight = 3.1 grams, mean $ERR\gamma^{+/+}$ body weight = 8.0 grams) and size (at p14 mean $ERR\gamma^{-/-}$ vertex-breech-length = 3.3cm, mean $ERR\gamma^{+/+}$ vertex-breech-length = 4.8cm).

- Nervous System

After it's removal from the neurocranium the $ERR\gamma^{+/+}$ and $ERR\gamma^{-/-}$ brains were gross anatomically indistinguishable. However, $ERR\gamma^{-/-}$ brains could be easily identified: the telencephalic region was shortened, with the lamina quadrigemina protruding at a greater extend between it and the cerebellar region (fig. 22). No other changes were observed between the three genotypes during their macroscopic assessment.

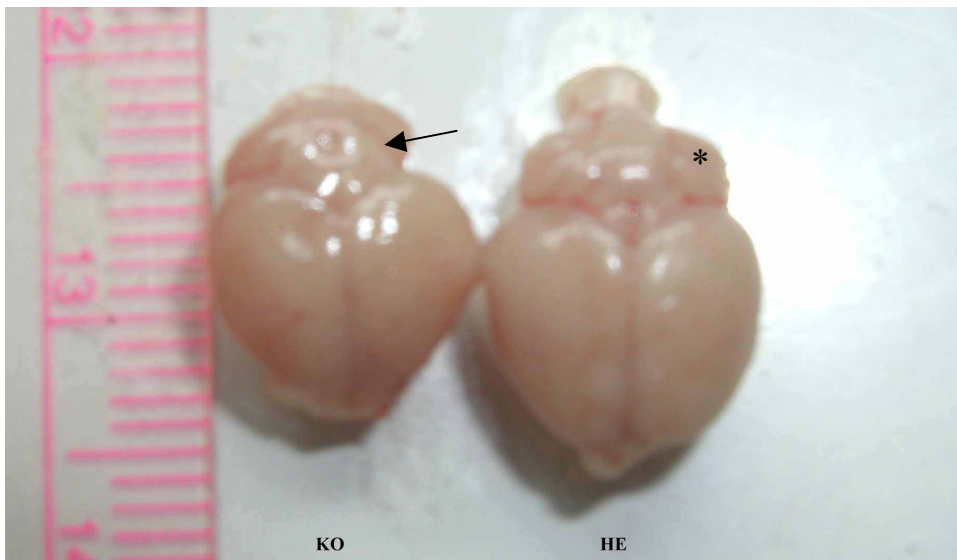


Fig. 22 Brains of an adult $ERR\gamma^{-/-}$ and a $ERR\gamma^{+/-}$ littermate pair. The telencephalic cortex of the $ERR\gamma^{-/-}$ is shortened dorsally, with the mesencephalic tegmentum (arrow) protruding to a greater extent between it and the cerebellar region compared to the appearance of the brain of its heterozygous littermate (asterisk).

- Gastrointestinal Tract

The distal esophagus, the stomach, the duodenum, the descendent colon and the liver were analyzed. The outer morphology of the $ERR\gamma^{+/+}$ and $ERR\gamma^{+/-}$ stomach did not reveal any structural changes, while the $ERR\gamma^{-/-}$ stomachs appeared enlarged, with distended walls, especially at the gastric corpus and antrum and had a hard consistence in comparison to their littermates (fig. 23a). These stomachs were sagittally divided into two pieces along the length of the greater and the lesser curvature into two slices. The inner stomach wall of the $ERR\gamma^{-/-}$ appeared thickened with protruding bulgy masses, which occupied to a great extent the organ's lumen (fig. 23b). No further macroscopic changes were observed at any of the other gastrointestinal organs.

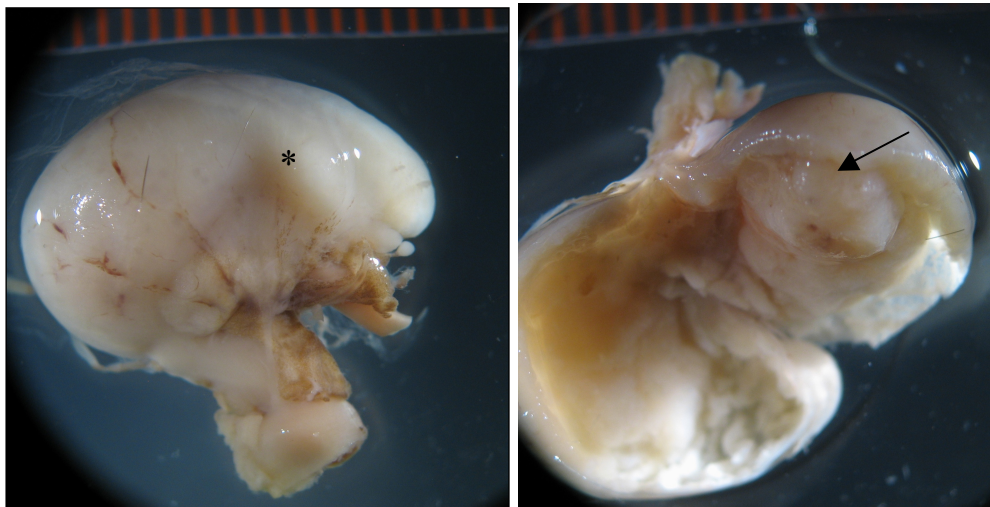


Fig. 23 a. Macroscopic appearance of a stomach of a $ERR\gamma^{-/-}$ adult mouse. Note the protruding mass of the gastric corpus (asterisk). b. After a sagittal section a clearer view of the protruding tumorous mass of the inner stomach wall at the level of the corpus (arrow).

- Urinary Tract

The kidneys of five of the acquired triplets were removed and examined. At all three genotypes they appeared to share a common morphology without any structural changes. Additionally, the urinary bladder of one triplet was removed and assessed. The outer appearances of all three genotypes' organs were not indicative of any morphological changes.

- Cardiovascular System

From one triplet the heart was also removed and assessed for pathological changes, without any being revealed at the macroscopic level.

- Spleen

The spleens of 5 adult triplets were removed and studied. None of them indicated any gross pathology, with the exception of one $ERR\gamma^{-/-}$ spleen, which in comparison was twice the size of the $ERR\gamma^{+/+}$ one.

- Respiratory System

The lungs of 5 adult triplets were examined. There were no structural changes observed between any of the three genotypes.

4.8 Histology

- Nervous System

A. Hematoxylin Eosin

All three genotypes looked identical and no pathological findings were observed.

B. Nissl Staining

Again, no differences between the three genotypes were obvious.

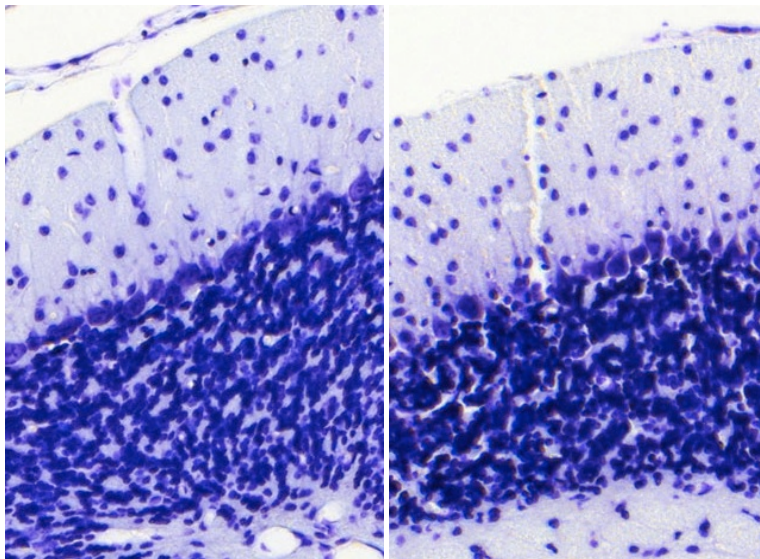


Fig. 24 Cerebellar cortex, Nissl Staining. The three-layered cortical structure of the cerebellum (stratum moleculare – SM, stratum purkinjiese – SP, stratum granulare – SG) can be seen without any pathological changes. $ERR\gamma^{+/+}$ left, $ERR\gamma^{-/-}$ right.

C. Kluever-Barrera staining

No significant qualitative differences between the three genotypes both in the myelin sheaths' density and distribution patterns, as well as in the cellular components analyzed could be observed.

- Gastrointestinal Tract

A. Hematoxylin Eosin

The stomachs of three adult triplets were removed and histologically assessed. Compared to the $ERR\gamma^{+/+}$ stomach, the $ERR\gamma^{-/-}$ stomach was hypertrophic and demonstrated hyperkeratosis of the epithelium with mitosis and non-infiltrative, papillary formations (keratohyalin bodies) and hypertrophy of the muscular layer. Additionally, glandular hypertrophy with occasional infiltration of mononuclear cells was observed (fig.26).

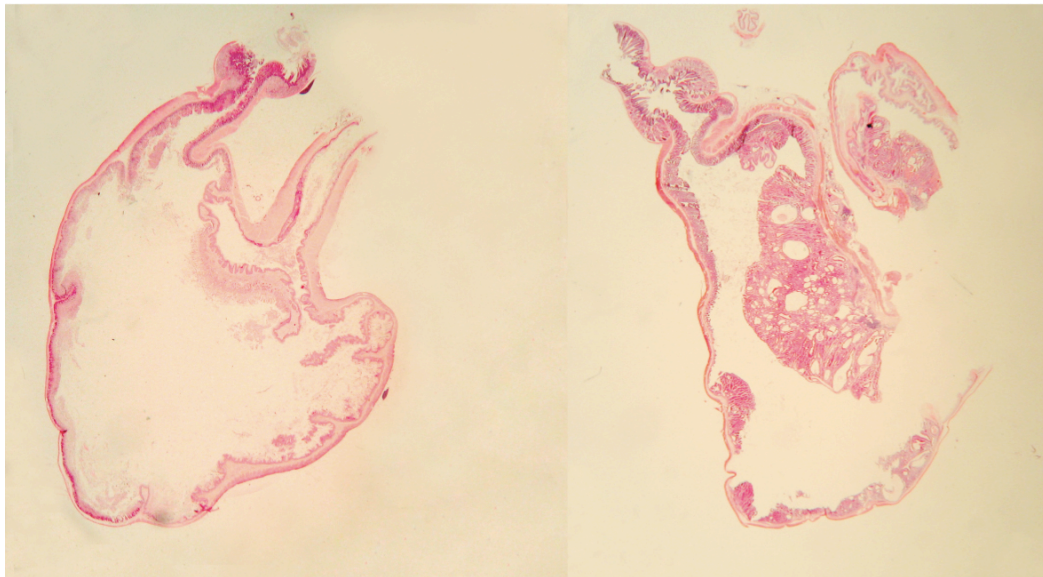


Fig. 25 Hematoxylin Eosin stain of a $ERR\gamma^{+/+}$ (left) and a $ERR\gamma^{-/-}$ (right) stomach. Prominent differences are observed in the $ERR\gamma^{-/-}$ stomach, with epithelial hypertrophy and hyperkeratosis, with formation of keratohyalin bodies and glandular hypertrophy with occasional mononuclear cell infiltration.

No pathological alteration was observed in any of the other assessed organs (distal esophagus, duodenum, descendent colon and liver).

Cardiovascular System

A. Hematoxylin Eosin

Under light microscopy the $ERR\gamma^{+/+}$ heart demonstrated a normal histology of all three cardiac layers (epicardium, myocardium and endocardium) without signs of any morphological abnormalities. Similarly, compared to their WT littermate, no qualitative differences were observed at the hearts of the HE and the $ERR\gamma^{-/-}$ mice.

4.8.1 Immunohistochemical examination of the $ERR\gamma$ triples

Nervous System

A. Glial Fibrillary Acid Protein

The hemispheres of two adult triplets were assessed for this study on sagittal sections; additionally one triplet and one diplet ($ERR\gamma^{+/+}$ and $ERR\gamma^{-/-}$ were also assessed on coronal sections.

In all examined regions, in both plane views of the astrocytic morphology (round to oval, partially triangular cellular body, with three to six main dendrites and rich further arborization) and their distribution frequency was alike. No astrogliosis, with the characteristic cellular hypertrophy, astrocytes proliferation and process extension (35) was observed at any of the examined brains.

B. Tyrosine Hydroxylase

TH-positive neurons were observed at the olfactory bulb (periglomerular cells), at diencephalic and hypothalamic groups (e. g. ventral tegmental area), at the mesencephalic tectum (substantia nigra) and at the medulla oblongata. Sporadic TH-positive fibers were seen at the cerebellar cortex. There were no qualitative or quantitative differences seen between the three genotypes concerning the distribution and morphology of the TH-immunoreactive regions (neurons and neuropil).

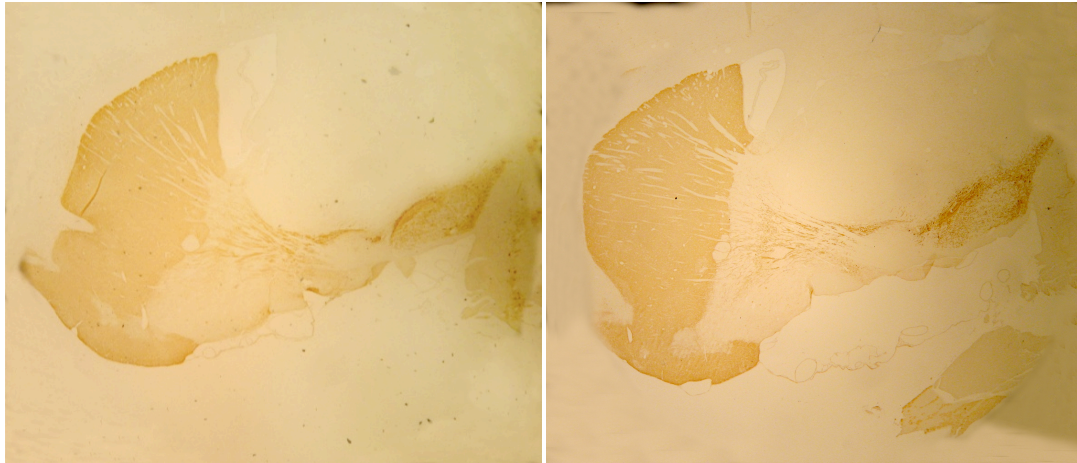


Fig. 26 Sagittal view of the Substantia nigra Pars compacta and Pars reticulata of the $ERR\gamma^{+/+}$ (left) and the $ERR\gamma^{-/-}$ (right). There were no morphological changes between the two genotypes in the distribution pattern of their long TH-immunoreactive fiber bundles crossing the diencephalon between the thalamic and the subthalamic area reaching the striatum observed.

4.9 Morphometry

4.9.1 The $ERR\gamma^{-/-}$ has a relative bigger mesencephalic tegmentum compared to the $ERR\gamma^{+/+}$, even though its absolute brain size is reduced

Figures 28 to 30 demonstrate the average values of the total brain size and the assessed brain regions between the $ERR\gamma^{+/+}$ and their $ERR\gamma^{-/-}$ littermates.

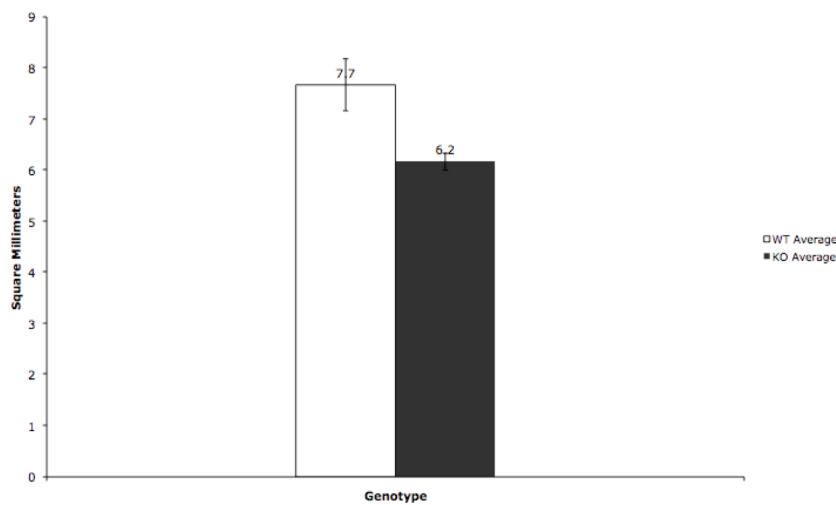


Fig. 27 Average total brain size for the $ERR\gamma^{+/+}$ [7.7 mm² (SEM= 0.51)] and the $ERR\gamma^{-/-}$ [6.2 mm² (SEM=0.16)] populations with SEM. There is a significant reduction (18.6%) in the $ERR\gamma^{-/-}$ brain size in comparison to the WT. $P < 0.05$

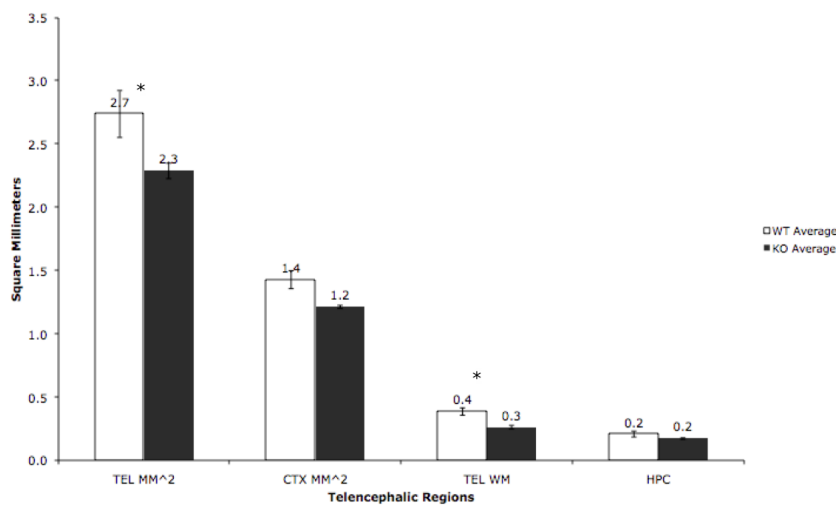


Fig. 28 Average values of the size of the telencephalon (TEL) and the telencephalic subregions [the telencephalic cortex (CTX), the telencephalic white matter (TEL WM)]

and the hippocampus (HPC)] for the $ERR\gamma^{+/+}$ and the $ERR\gamma^{-/-}$ populations measured in square millimeters with SEM. Regions showing significant differences in size are the *telencephalon* [$ERR\gamma^{+/+} = 2.74 \text{ mm}^2$ (SEM= ± 0.19), $ERR\gamma^{-/-} = 2.29 \text{ mm}^2$ (SEM= ± 0.06)] and the *telencephalic white matter* [$ERR\gamma^{+/+} = 0.39 \text{ mm}^2$ (SEM= ± 0.03), $ERR\gamma^{-/-} = 0.27 \text{ mm}^2$ (SEM= ± 0.01)] (*). $P < 0.05$

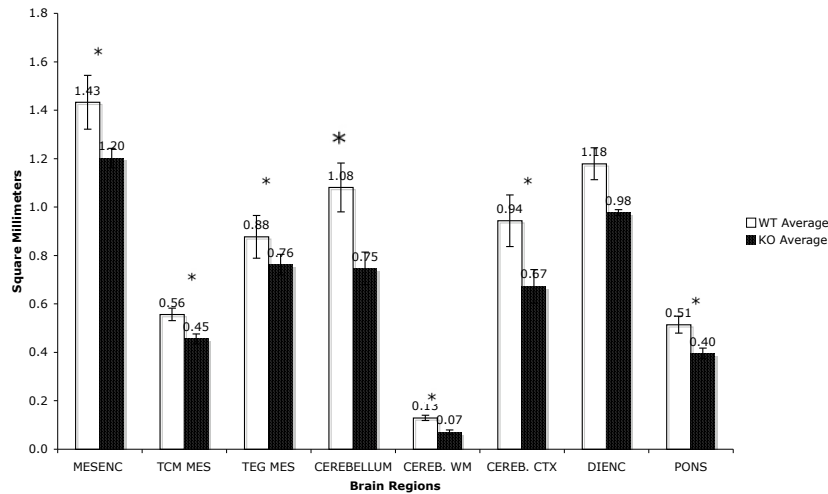


Fig. 29 Average values of the size of the mesencephalon (MESENC) and the mesencephalic subregions [the mesencephalic tectum (TCM MES), the mesencephalic tegmentum (TEG MES), the cerebellum (CEREBELLUM), the cerebellar white matter (CEREB. WM.), the cerebellar cortex (CEREB. CTX), the diencephalon (DIENC) and the pons (PONS) with SEM. Significant differences in size of the assessed regions are shown between the *mesencephalon* [$ERR\gamma^{+/+} = 1.4 \text{ mm}^2$ (SEM= ± 0.11), $ERR\gamma^{-/-} = 1.2 \text{ mm}^2$ (SEM= ± 0.04)], the *mesencephalic tectum* [$ERR\gamma^{+/+} = 0.56 \text{ mm}^2$ (SEM= ± 0.02), $ERR\gamma^{-/-} = 0.45 \text{ mm}^2$ (SEM= ± 0.02)], the *cerebellum* [$ERR\gamma^{+/+} = 1.1 \text{ mm}^2$ (SEM= ± 0.1), $ERR\gamma^{-/-} = 0.75 \text{ mm}^2$ (SEM= ± 0.07)], the *cerebellar white matter* [$ERR\gamma^{+/+} = 0.13 \text{ mm}^2$ (SEM= ± 0.01), $ERR\gamma^{-/-} = 0.07 \text{ mm}^2$ (SEM= ± 0.001)] and *cortex* [WT= 0.94 mm^2 (SEM= ± 0.1), $ERR\gamma^{-/-} = 0.67 \text{ mm}^2$ (SEM= ± 0.07)] and the *pons* [$ERR\gamma^{+/+} = 0.51 \text{ mm}^2$ (SEM= ± 0.03), $ERR\gamma^{-/-} = 0.4 \text{ mm}^2$ (SEM= ± 0.02)]. (*). $P < 0.05$

The average value of the $ERR\gamma^{-/-}$ mouse total brain size was 6.2 mm^2 (SEM=0.16), significantly reduced by 18.6% in comparison to the $ERR\gamma^{+/+}$ value 7.7 mm^2 (SEM= 0.51). Whereas all the brain regions of the $ERR\gamma^{-/-}$ are reduced in size compared to the

WT, the ones, which showed a significant (*) size reduction as shown at figures 29 and 30 are telencephalon, telencephalic white matter, mesencephalon, mesencephalic tectum, the cerebellum, cerebellar white matter, cerebellar cortex and pons.

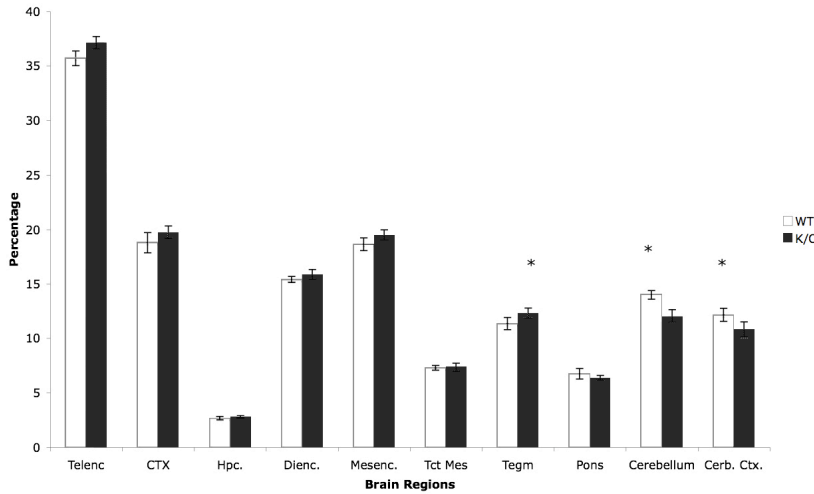


Fig. 30 Genotypic differences in brain region size between the $ERR\gamma^{+/+}$ and the $ERR\gamma^{-/-}$ littermate mice. The average values of the brain regions normalized to the genotype's total brain size for the $ERR\gamma^{+/+}$ and $ERR\gamma^{-/-}$ populations with SEM are shown. Regions showing significant differences in size (*) are the *mesencephalic tegmentum* (11.35% [SEM= ± 0.56] for the $ERR\gamma^{+/+}$ and 12.32% [SEM= ± 0.46] for the $ERR\gamma^{-/-}$), the *cerebellum* (14% [SEM= ± 0.39] for the $ERR\gamma^{+/+}$ and 12.03% [SEM= ± 0.73] for the $ERR\gamma^{-/-}$) and the *cerebellar cortex* (12.16% [SEM= ± 0.16] for the $ERR\gamma^{+/+}$ and 10.92% [SEM= ± 0.81] for the $ERR\gamma^{-/-}$). $P < 0.05$ between groups.

As shown in figure 31 the normalized to the genotype values of the brain regions were significantly different in three regions. The mesencephalic tegmentum of the $ERR\gamma^{-/-}$ was significantly bigger in size than the $ERR\gamma^{+/+}$ one (11.35% [SEM= ± 0.56] for the $ERR\gamma^{+/+}$ and 12.32% [SEM= ± 0.46] for the $ERR\gamma^{-/-}$). On the other hand, the $ERR\gamma^{-/-}$ cerebellum (14% [SEM= ± 0.39] for the $ERR\gamma^{+/+}$ and 12.03% [SEM= ± 0.73] for the $ERR\gamma^{-/-}$) and the cerebellar cortex (12.16% [SEM= ± 0.16] for the $ERR\gamma^{+/+}$ and 10.92% [SEM= ± 0.81] for the $ERR\gamma^{-/-}$) were significantly reduced compared to the $ERR\gamma^{+/+}$ ones.

The $ERR\gamma^{+/-}$ mice showed no significant differences when compared to their $ERR\gamma^{+/+}$ littermates, in terms of their absolute and normalized total brain size and of their assessed brain regions.

5. DISCUSSION

The present study has been undertaken in order to assess the function of the ERR γ by examining the effects of its loss using ERR $\gamma^{-/-}$ mice. Weight and vertex-breech-length development, behavioral analysis of the adult animals and histological studies were conducted in order to examine whether any structural pathological differences were present between ERR $\gamma^{+/+}$, heterozygous and homozygous ERR $\gamma^{-/-}$ mice.

Pre- and Post-Natal Development

First of all, we observed that there was a post-natal underrepresentation (P1: 15.6% ERR $\gamma^{+/+}$, 75% ERR $\gamma^{+/-}$, 9.4% ERR $\gamma^{-/-}$, P3 42.3% ERR $\gamma^{+/+}$, 50% HE, 7.7% ERR $\gamma^{-/-}$) in the knockout litter mice compared to the two control groups. This observation indicates an increased lethality of the homozygous ERR $\gamma^{-/-}$ mice phenotype, demonstrating a functional role of the ERR γ in survival. This finding is consistent with the work of Alaynick et al. (36), who showed that ERR $\gamma^{-/-}$ mice died during the first week of life. Alaynick et al. (36) analyzed the role of the ERR γ in the pathophysiological development of the mutant mice and demonstrated that the loss of ERR γ blocks the transition from a predominant dependence on carbohydrates as substrates during the fetal period to a greater dependence on oxidative metabolism in postnatal life causing lactatemia, electrocardiogram abnormalities, high mitochondrial genome number and altered electron transport chain biochemical activities. Although no weight reduction of our ERR $\gamma^{-/-}$ mice occurred during pre-natal development in comparison to the ERR $\gamma^{+/+}$ mice indicating that the ERR $\gamma^{-/-}$ did not have any effect on the surviving animals, however, weight reduction on days P1, P3 and P14 of 23.5 %, 20% and 63.1% respectively was observed. This observation is again consistent with the data of Alaynick et al. (36) who also demonstrated that the ERR $\gamma^{-/-}$ body weight was significantly lower than the ERR $\gamma^{+/+}$ littermate controls. Moreover, we showed that the vertex-breech length of the ERR $\gamma^{-/-}$ mice was progressively reduced during post-natal development compared to the control group.

These findings are coherent to the hypothesis that the lack of the ERR γ affects basic metabolic functions.

Adult ERR γ knockouts

Whereas in the only existing study to date (36), which examined ERR γ ^{-/-} mice, none of the mice survived longer than P7, and in the current work under 1% of the generated ERR γ ^{-/-} reached adulthood. As demonstrated, these mice weighed 58.6 % of their ERR γ ^{+/+} littermate controls and were 87.3% as long, which is furthermore indicative of a significant - but not as in the work of Alaynick et al. (36) - absolute lethal disruption in the metabolic function of their organisms. This discrepancy between the findings of Alaynick and the data presented in this study can be explained by considering the data of Dufour et al. (37). Using a combination of chromatin immunoprecipitation (ChIP) and genomic DNA arrays (ChIP-on-chip), they identified the target promoters (ERR response element – ERRE) of the ERR α and ERR γ . The ERRE showed a significant overlap between the two, regulating common biological processes in the tissue when co-expressed (uptake and cytoplasmatic processing of energy substrates; the production of Adenosine-5'-triphosphate (ATP) via glucose and fatty acid oxidation; the tricarboxylic acid cycle and oxidative phosphorylation; the transport of ATP across the mitochondrial membranes and generation of the phosphocreatine pool by creatine kinase; and the sensing of cellular energy charge through the Serine/threonine kinase 11, adenine monophosphate-activated protein kinase, acetyl-CoA carboxylase-2 isoform, Malonyl CoA decarboxylase - LKB1/AMPK/ACC2, MCD - pathway and Ca⁺² handling and contractile work). Furthermore he showed that the nicotinamide adenine dinucleotide (NADH) dehydrogenase ubiquinone 1 beta subcomplex 5 (Ndufb5), a component of the oxidative phosphorylation pathway was up-regulated approximately 50% in ERR γ ^{-/-}, suggesting compensation through increased ERR α expression and discussed the possibility of a broad genetic program regulation essential for proper heart function in which the three ERR isoforms act in concert. Therefore the co-orchestration of the metabolic functions by all three ERRs could lead to the viable compensation of the loss of the ERR γ ^{-/-} in terms of a salvage pathway, through the up-regulation of transcriptional regulators of mitochondrial function (e.g. Peroxisome proliferator-activated receptor-gamma coactivator 1alpha -PGC-1a-, ERR α and Nuclear erythroid 2 p45-related factor 2 - NRF-2).

The ERR γ Brain

Lorke et al. (31) detected by in situ hybridization the expression of the ERR γ in the adult murine brain, which was abundantly present mostly in the mesencephalic (with strong signaling in all three main dopaminergic regions, the retrorubral field, substantia nigra and the ventral tegmental area) and hindbrain regions, but was also expressed in the cerebellum (deep cerebellar nuclei, interneurons of the molecular layer and Golgi cells of the granular layer). Since the gross anatomical appearance of the ERR γ ^{-/-} differed from the heterozygote and wildtype controls with respect to a dorsally shortened telencephalic region and to a lamina quadrigemina protruding to a greater extent between the telencephalon and the cerebellum, a morphometric analysis of different brain regions was performed. It showed that the size of the mesencephalic tegmentum (normalized to the total brain size) of the ERR γ ^{-/-} was bigger (11.35% [SEM= \pm 0.56]) than the size of the corresponding ERR γ ^{+/+} brain region (12.32% [SEM= \pm 0.46]). On the other hand the normalized value of the size of the cerebellum and the cerebellar cortex of the ERR γ ^{-/-} were significantly reduced compared to the ERR γ ^{+/+} (12.03% [SEM= \pm 0.73], 10.92% [SEM= \pm 0.81] and (14% [SEM= \pm 0.39], (12.16% [SEM= \pm 0.16] - ERR γ ^{-/-} and ERR γ ^{+/+} cerebellum and cerebellar cortex size, respectively).

When the distribution pattern of the ERR γ with the ERR α was compared [Bonnelye et al. (38)], it was shown there is an overlapping and complex, but distinguishable, pattern in the expression of the two receptors. According to the experiments of Bardet et al. (26) all ERR genes were found co-expressed in groups of neurons in the rhombomeres of the hindbrain during development in a temporal sequence of appearance: first ERR γ , then ERR β and finally ERR α . These findings in the mouse reflected similar findings in zebrafish development, where the inhibition of the ERR α in the very early stages of zebrafish development (1 to 4 cells), led to a severe delay in cellular movements that precede and are necessary to gastrulation (39). Additionally, utilizing the data of Liu et al. (40) and Zhang (41) et al. who showed that the ERR γ enhanced by the coactivator PGC-1 α activates the multi-hormone-response element (MHRE) of the ERR α , the research team of Bardet postulated the hypothesis that there is a cross-regulation of the expression of these receptors and that they comprise a conserved marker of cellular/molecular segmentation even when this has not yet appeared in evolution (27). Finally, the hypothesis that the ERR γ possesses a crucial role in murine neurogenesis is

supported by the pattern of its expression during embryogenesis, which starting from E10.5 to E16.5 showed enhanced signals of the receptor primary in the mesencephalic, cerebellar and metencephalic regions, which is in line to a neural migration disruption affecting the morphometrically disproportional areas observed in this study (32).

Both in $ERR\alpha^{-/-}$ and $ERR\gamma^{-/-}$ mice, no cytomorphological differences were observed under light microscopy (induced apoptosis, neurodegeneration, astrogliosis or inflammatory response).

Movement Disorders

The regulation of movement in mammals is an extremely complex process, which requires a perfect interaction between virtually all cortical and subcortical areas. The failure of this optimal interaction due to anatomical and/or functional causes results to a broad pattern of movement disorders. Movement disorders are classified as either hyperkinetic (myoclonus, chorea, ballism, tics, dystonia) or hypokinetic (parkinsonism). The term dystonia was first described in 1911 by Oppenheim and Vogt for a childhood-onset syndrome consisting of twisted postures, muscle spasms, bizarre walking, with bending and twisting of the torso, rapid, sometimes-rhythmic jerking movement and progression of symptoms eventually leading to sustained fixed postural deformities (42). In his work in 1988 - the concept and classification of dystonia - Fahn (43) defined dystonia more precisely as a disorder of movement caused by involuntary sustained muscle contractions affecting one or more sites of the body, frequently causing twisting and repetitive movement or abnormal postures.

A vast majority of data indicates that both the basal ganglia and the cerebellum possess key roles in the pathophysiology of dystonia (44-48). Delineating the role of the cerebellum in this pathological process, Campbell et al. (49, 50) showed in mutant tottering mice that abnormal cerebellar output is essential for the generation of dystonic movements. Furthermore, surgical removal of the cerebellum in these mutants eliminated dystonia (51), while the induction of toxic damage to the cerebellum in healthy mice also leads to a dystonic phenotype (52).

Based on this data it could be hypothesized that the significantly smaller cerebellar size of the mutant $ERR\gamma$ mice in comparison to their wildtype littermate controls, even in the absence of cellular pathology under light microscopy, should lead to a dysfunctional motor-control output, which in turn would be (co-)responsible for the severely dystonic phenotype of the examined mice.

The second region of interest, the mesencephalic tegmentum of the ERR γ mice with the substantia nigra and its direct projections to the striatum plays a significant role in the pathogenesis of many extrapyramidal disorders, such as parkinson's disease (53, 54) and as already mentioned above in certain forms of dystonia. After labeling the dopaminergic neurons with tyrosine hydroxylase both in sagittal and frontal layers, no numerical or qualitative abnormalities were found between the three genotypes, indicating either a primarily functional disruption of the substantia nigra –or a morphological one at an ultrastructural level - or an additional morphological and functional breaching between the cerebellum and the basal ganglia, the two basic dystonia generators, upon receptor loss.

Gastric Tumors

The crucial role of the ERR γ in cell proliferation of different tissues has been demonstrated in various publications so far (for review see 55). However, what remains undetermined is the exact function of the receptor, since existing data support both the role of a tissue-specific promoter or suppressor of proliferation. On one hand it has been demonstrated for all ERRs that their interaction with the hypoxia-inducible-factor (HIF) leads to transcriptional activation of hypoxic genes promoting solid-tumor growth such as gastric cancer (56-58). On the other hand, it has been shown that the presence of ERR γ in prostatic cancer cells significantly suppresses tumorigenicity and could be a novel therapeutic target for prostate cancer treatment (59). Similarly, this favorable anti-proliferative role of the ERR γ was also shown for the ovaries (60), where ovarian cancer was suppressed. Concerning breast tissue the receptor plays an enigmatic role, which remains yet to be unraveled, since data support both a beneficial as well as an adverse effect on cell-proliferation (61, 62).

The prominent gastric glandular hyperplasia witnessed at the ERR γ ^{-/-} mice in this work indicates that the receptor, strongly expressed in the stomach (63) acts as a suppressor of uncontrolled glandular cell proliferation and its lack leads to tumor formation. This could potentially take place through the induction of the transcriptional coactivator PGC-1 α , as already mentioned above, which in turn promotes angiogenesis and cell proliferation through the ERRA. Nevertheless this has been demonstrated so far only for myotubes under vivo conditions (64). Another possibility could be that the tissue-specific interplay between estrogen related receptor gamma and the estrogen receptors, for which an unclear but certain role has already been demonstrated in gastric

tumorigenesis (65, 66) could lead to this uncontrolled benign glandular cell proliferation, in a complex mechanism, which still remains to be resolved.

One receptor, one mouse model and so many functions

In order to understand the function of the ERR γ more precisely, certain actions should be undertaken in further study. First, the examination of a larger cohort is crucial in order to achieve statistically significant results, which will boost the informational level from mostly descriptive to quantitative one.

Second, developmental studies concerning the murine brain should be performed in order to define the very first moments of the appearance of morphological abnormalities. Neurophysiological testing such as electroencephalography and electromyography will detect functional anomalies (epileptogenic potentials, chorea, myoclonus, tremor) in the mice leading to a more precise characterization of the phenotype and its pathophysiology. Furthermore larger populations will also allow the quantitative evaluation of the morphometric size and the cellular density of the mesencephalic substantia nigra, labeled with the tyrosine-hydroxylase antibody, which did not present any differences at microscopical examination alone. Additionally parvalbumin immunohistochemistry should be performed in order to allow the evaluation of the GABAergic neurons, specific morphological changes of which have been demonstrated for other dystonia mouse models (67, 68). Additional regions, such as the basal ganglia should also be more precisely evaluated (morphometrical size of each nucleus), since they play a paramount role in dystonia and since a neuroprotective role of these neurons has been shown for the PGC-1 α (69), which is potentially mediated through interplay with the ERR γ . Finally, depending on the findings of the above mentioned additional studies, medication could be given (dopaminergic, anticholinergic, antiepileptic) in order to evaluate significant changes in the performance of the animals. neu

Similarly for the stomach, histological analysis throughout development in larger populations would allow to define the beginning of the tumorigenic process and identifying its first pathological changes. Additionally blood analyses should be performed (e. g. protein electrophoresis) in order to reveal aberrations [hypoalbuminemia in the case of menetrier's disease, which is characterized by giant gastric folds, foveolar hyperplasia and various degrees of inflammatory infiltration

(70)], which could lead to a better characterization of the phenotype and pathophysiological understanding.

It has become apparent that the $ERR\gamma$ plays a key role in metabolic functions, cell proliferation and brain development. Certainly these functions are not controlled solely by the $ERR\gamma$, but through a complex interaction with the $ERR\alpha$, the estrogen receptors and other activation cofactors (such as PGC-1a). The elicitation of this perplex functionality can only be achieved through a fine co-orchestration between all these factors, the exact mechanisms of which are still not fully comprehended and are under intensive research.

REFERENCES

1. Laudet V and Gronemeyer H (2002) *The Nuclear receptor Facts Book*, Academic Press, San Diego.
2. Jensen EV (1962) On the mechanism of estrogen action. *Perspect Biol Med* 6: 47-59.
3. Germain, P., B. Staels, et al. (2006). "Overview of nomenclature of nuclear receptors." *Pharmacol Rev* 58: 685-704.
4. (1999). "A unified nomenclature system for the nuclear receptor superfamily." *Cell* 97: 161-3.
5. Laudet, V. (1997). "Evolution of the nuclear receptor superfamily: early diversification from an ancestral orphan receptor." *J Mol Endocrinol* 19: 207-26.
6. Giguere, V. (1999). "Orphan nuclear receptors: from gene to function." *Endocr Rev* 20: 689-725.
7. Wurtz, J. M., W. Bourguet, et al. (1996). "A canonical structure for the ligand-binding domain of nuclear receptors." *Nat Struct Biol* 3: 87-94.
8. Aranda, A. and A. Pascual (2001). "Nuclear hormone receptors and gene expression." *Physiol Rev* 81: 1269-304.
9. Horlein, A. J., A. M. Naar, et al. (1995). "Ligand-independent repression by the thyroid hormone receptor mediated by a nuclear receptor co-repressor." *Nature* 377: 397-404.
10. Chen, J. D. and R. M. Evans (1995). "A transcriptional co-repressor that interacts with nuclear hormone receptors." *Nature* 377: 454-7.
11. Sap, J., A. Munoz, et al. (1989). "Repression of transcription mediated at a thyroid hormone response element by the v-erb-A oncogene product." *Nature* 340: 242-4.
12. Graupner, G., K. N. Wills, et al. (1989). "Dual regulatory role for thyroid-hormone receptors allows control of retinoic-acid receptor activity." *Nature* 340: 653-6.

13. Wolffe, A. P. (1997). "Transcriptional control. Sinful repression." *Nature* 387: 16-7.
14. Hentschke, M., U. Susens, et al. (2002). "Domains of ERRgamma that mediate homodimerization and interaction with factors stimulating DNA binding." *Eur J Biochem* 269: 4086-97.
15. Benoit, G., A. Cooney, et al. (2006). "International Union of Pharmacology. LXVI. Orphan nuclear receptors." *Pharmacol Rev* 58: 798-836.
16. Giguere, V., N. Yang, et al. (1988). "Identification of a new class of steroid hormone receptors." *Nature* 331: 91-4.
17. Gu, P., D. LeMenuet, et al. (2005). "Orphan nuclear receptor GCNF is required for the repression of pluripotency genes during retinoic acid-induced embryonic stem cell differentiation." *Mol Cell Biol* 25: 8507-19.
18. Watt, A. J., W. D. Garrison, et al. (2003). "HNF4: a central regulator of hepatocyte differentiation and function." *Hepatology* 37: 1249-53.
19. Bonnelye, E., J. M. Vanacker, et al. (1997). "The ERR-1 orphan receptor is a transcriptional activator expressed during bone development." *Mol Endocrinol* 11: 905-16.
20. Luo, J., R. Sladek, et al. (1997). "Placental abnormalities in mouse embryos lacking the orphan nuclear receptor ERR-beta." *Nature* 388: 778-82.
21. Inoue, I., Y. Shinoda, et al. (2005). "CLOCK/BMAL1 is involved in lipid metabolism via transactivation of the peroxisome proliferator-activated receptor (PPAR) response element." *J Atheroscler Thromb* 12: 169-74.
22. Eudy, J. D., S. Yao, et al. (1998). "Isolation of a gene encoding a novel member of the nuclear receptor superfamily from the critical region of Usher syndrome type IIa at 1q41." *Genomics* 50: 382-4.

23. Hong, H., L. Yang, et al. (1999). "Hormone-independent transcriptional activation and coactivator binding by novel orphan nuclear receptor ERR3." *J Biol Chem* 274: 22618-26.
24. Heard, D. J., P. L. Norby, et al. (2000). "Human ERRgamma, a third member of the estrogen receptor-related receptor (ERR) subfamily of orphan nuclear receptors: tissue-specific isoforms are expressed during development and in the adult." *Mol Endocrinol* 14: 382-92.
25. Sullivan, A. A. and C. S. Thummel (2003). "Temporal profiles of nuclear receptor gene expression reveal coordinate transcriptional responses during *Drosophila* development." *Mol Endocrinol* 17: 2125-37.
26. Bardet, P. L., M. Schubert, et al. (2005). "Expression of estrogen-receptor related receptors in amphioxus and zebrafish: implications for the evolution of posterior brain segmentation at the invertebrate-to-vertebrate transition." *Evol Dev* 7: 223-33.
27. Bardet, P. L., V. Laudet, et al. (2006). "Studying non-mammalian models? Not a fool's ERRand!" *Trends Endocrinol Metab* 17: 166-71
28. Pettersson, K., K. Svensson, et al. (1996). "Expression of a novel member of estrogen response element-binding nuclear receptors is restricted to the early stages of chorion formation during mouse embryogenesis." *Mech Dev* 54: 211-23.
29. Tremblay, G. B., D. Bergeron, et al. (2001). "4-Hydroxytamoxifen is an isoform-specific inhibitor of orphan estrogen-receptor-related (ERR) nuclear receptors beta and gamma." *Endocrinology* 142: 4572-5.
30. Bookout, A. L., Y. Jeong, et al. (2006). "Anatomical profiling of nuclear receptor expression reveals a hierarchical transcriptional network." *Cell* 126: 789-99.
31. Lorke, D. E., U. Susens, et al. (2000). "Differential expression of the estrogen receptor-related receptor gamma in the mouse brain." *Brain Res Mol Brain Res* 77: 277-80.

32. Hermans-Borgmeyer, I., U. Susens, et al. (2000). "Developmental expression of the estrogen receptor-related receptor gamma in the nervous system during mouse embryogenesis." *Mech Dev* 97: 197-9.
33. Tremblay, A. M. and V. Giguere (2007). "The NR3B subgroup: an ovERRview." *Nucl Recept Signal* 5: e009
34. Sidman, R. L., Angevine, J. B., Jr & Taber Pierce, E. *Atlas of the Mouse Brain and Spinal Cord* (Harvard University Press, Cambridge, Massachusetts 1971)
35. Ridet, J. L., S. K. Malhotra, et al. (1997). "Reactive astrocytes: cellular and molecular cues to biological function." *Trends Neurosci* 20: 570-7.
36. Alaynick WA, Kondo RP, Xie W, He W, Dufour CR, Downes M, Jonker JW, Giles W, Naviaux RK, Giguère V, Evans RM. C (2007) ERRgamma directs and maintains the transition to oxidative metabolism in the postnatal heart. *Cell Metabol.* 6:13-24
37. Dufour CR, Wilson BJ, Huss JM, Kelly DP, Alaynick WA, Downes M, Evans RM, Blanchette M, Giguère V. Genome-wide orchestration of cardiac functions by the orphan nuclear receptors ERR alpha and gamma. *Cell Metab.* 2007 5:345-56
38. Bonnelye E, Vanacker JM, Spruyt N, Alric S, Fournier B, Desbiens X, Laudet V. Expression of the estrogen-related receptor 1 (ERR-1) orphan receptor during mouse development. *Mech Dev.* 1997 65:71-85.
39. Bardet PL, Horard B, Laudet V, Vanacker JM. The ERRalpha orphan nuclear receptor controls morphogenetic movements during zebrafish gastrulation. *Dev Biol.* 2005 281:102-11.
40. Liu D, Zhang Z, Teng CT. Estrogen-related receptor-gamma and peroxisome proliferator-activated receptor-gamma coactivator-1alpha regulate estrogen-related receptor-alpha gene expression via a conserved multi-hormone response element. *J Mol Endocrinol.* 2005 34:473-87.

41. Zhang Z, Teng CT. Interplay between estrogen-related receptor alpha (ERRalpha) and gamma (ERRgamma) on the regulation of ERRalpha gene expression. *Mol Cell Endocrinol.* 2007 264:128-41. Epub 2006 Dec 8.
42. Openheim Ueber eine eigenartige Krampfkrankheit des kindlichen und jugendlichen Alters (Dysbasia lordotica progressiva, Dystonia musculorum deformans)
43. Fahn, S. (1988). "Concept and classification of dystonia." *Adv Neurol* 50: 1-8.
44. Marsden, C. D., J. A. Obeso, et al. (1985). "The anatomical basis of symptomatic hemidystonia." *Brain* 108: 463-83.
45. Obeso JA, Gimenez-Roldan S. Clinicopathological correlation in symptomatic dystonia. In: Fahn S, editor. *Dystonia 2, Advances in Neurology*. New York: Raven Press; 1988. pp. 113–122.
46. Berardelli, A., J. C. Rothwell, et al. (1998). "The pathophysiology of primary dystonia." *Brain* 121: 1195-212.
47. Krauss, J. K., W. Seeger, et al. (1997). "Cervical dystonia associated with tumors of the posterior fossa." *Mov Disord* 12: 443-7.
48. LeDoux, M. S. and K. A. Brady (2003). "Secondary cervical dystonia associated with structural lesions of the central nervous system." *Mov Disord* 18: 60-9.
49. Campbell, D. B. and E. J. Hess (1998). "Cerebellar circuitry is activated during convulsive episodes in the tottering (tg/tg) mutant mouse." *Neuroscience* 85: 773-83.
50. Campbell, D. B., J. B. North, et al. (1999). "Tottering mouse motor dysfunction is abolished on the Purkinje cell degeneration (pcd) mutant background." *Exp Neurol* 160: 268-78.
51. Neychev, V. K., X. Fan, et al. (2008). "The basal ganglia and cerebellum interact in the

- expression of dystonic movement." *Brain* 131: 2499-509.
52. Pizoli, C. E., H. A. Jinnah, et al. (2002). "Abnormal cerebellar signaling induces dystonia in mice." *J Neurosci* 22: 7825-33.
53. Snyder, S. H. and R. J. D'Amato (1986). "MPTP: a neurotoxin relevant to the pathophysiology of Parkinson's disease. The 1985 George C. Cotzias lecture." *Neurology* 36: 250-8.
54. Bezard, E., C. Imbert, et al. (1998). "Experimental models of Parkinson's disease: from the static to the dynamic." *Rev Neurosci* 9: 71-90.
55. Ariazi, E. A. and V. C. Jordan (2006). "Estrogen-related receptors as emerging targets in cancer and metabolic disorders." *Curr Top Med Chem* 6: 203-15.
56. Ao, A., H. Wang, et al. (2008). "Involvement of estrogen-related receptors in transcriptional response to hypoxia and growth of solid tumors." *Proc Natl Acad Sci U S A* 105: 7821-6.
57. Quintero, M., N. Mackenzie, et al. (2004). "Hypoxia-inducible factor 1 (HIF-1) in cancer." *Eur J Surg Oncol* 30: 465-8.
58. Takahashi, R., S. Tanaka, et al. (2003). "Hypoxia-inducible factor-1alpha expression and angiogenesis in gastrointestinal stromal tumor of the stomach." *Oncol Rep* 10: 797-802.
59. Yu, S., X. Wang, et al. (2007). "ERRgamma suppresses cell proliferation and tumor growth of androgen-sensitive and androgen-insensitive prostate cancer cells and its implication as a therapeutic target for prostate cancer." *Cancer Res* 67: 4904-14.
60. Sun, P., J. Sehouli, et al. (2005). "Expression of estrogen receptor-related receptors, a subfamily of orphan nuclear receptors, as new tumor biomarkers in ovarian cancer cells." *J Mol Med* 83: 457-67.

61. Ariazi, E. A., G. M. Clark, et al. (2002). "Estrogen-related receptor alpha and estrogen-related receptor gamma associate with unfavorable and favorable biomarkers, respectively, in human breast cancer." *Cancer Res* 62: 6510-8..
62. Riggins, R. B., J. P. Lan, et al. (2008). "ERRgamma mediates tamoxifen resistance in novel models of invasive lobular breast cancer." *Cancer Res* 68(21): 8908-17.
63. Sanyal, S., J. Y. Kim, et al. (2002). "Differential regulation of the orphan nuclear receptor small heterodimer partner (SHP) gene promoter by orphan nuclear receptor ERR isoforms." *J Biol Chem* 277: 1739-48.
64. Arany, Z., S. Y. Foo, et al. (2008). "HIF-independent regulation of VEGF and angiogenesis by the transcriptional coactivator PGC-1alpha." *Nature* 451: 1008-12.
65. Chandanos, E., C. A. Rubio, et al. (2008). "Endogenous estrogen exposure in relation to distribution of histological type and estrogen receptors in gastric adenocarcinoma." *Gastric Cancer* 11: 168-74.
66. Kim, J. H., Y. J. Boo, et al. (2008). "Incidence and long-term outcome of young patients with gastric carcinoma according to sex: does hormonal status affect prognosis?" *Arch Surg* 143: 1062-7; discussion 1067.
67. Wahnschaffe, U., G. Fredow, et al. (1990). "Neuropathological studies in a mutant hamster model of paroxysmal dystonia." *Mov Disord* 5: 286-93.
68. Gernert, M., M. Hamann, et al. (2000). "Deficit of striatal parvalbumin-reactive GABAergic interneurons and decreased basal ganglia output in a genetic rodent model of idiopathic paroxysmal dystonia." *J Neurosci* 20: 7052-8..
69. McGill, J. K. and M. F. Beal (2006). "PGC-1alpha, a new therapeutic target in Huntington's disease?" *Cell* 127: 465-8.
70. Wolfsen, H. C., H. A. Carpenter, et al. (1993). "Menetrier's disease: a form of hypertrophic gastropathy or gastritis?" *Gastroenterology* 104: 1310-9

Index of figures

Fig. 1 Anatomy of nuclear receptors. The amino-terminal domain (A/B) domain, that contributes to ligand-independent activation of the receptor. The DNA-binding (C) domain, which leads to gene activation. The hinge region (D domain) bridging the C with the E domain and allowing conformational changes of the receptor. The ligand binding (E) domain through which homo- or hetero-dimerization after ligand binding is achieved and transcriptional activation or suppression is accomplished. The inconsistently appearing in some of the nuclear receptors C-terminal, (F domain), whose function is yet not fully understood. For information see text. [modified from Giguere (6)]	11
Fig. 2 Circular dendrogram depicting the relationship between nuclear receptor expression, function and physiology, revealing the major role of the nuclear receptors to reproduction, development, central and basal metabolic functions, dietary-lipid-metabolism and energy homeostasis. [from Bookout, A. L., Y. Jeong, et al. (30)].	13
Fig. 3 Brain areas measured and compared between the three genotypes. The total brain area (red), the telencephalic area (yellow), the diencephalon (blue), the mesencephalon (green), the cerebellum (purple) and the pons (grey) were analyzed.	27
Fig. 4 Southern Blot for the genotypic determination of the $ERR\gamma$ mice. <i>EcoRI</i> digested DNA of the genotypes indicated was separated on a 0.8% agarose gel and subjected to Southern blotting. For detection a ^{32}P -dATP labeled 3` of the homology region was used and a Fujix BAS Reader for the visualization of the signals. $ERR\gamma^{+/-}$ (+/-, left) displayed an upper wild type signal at 15 kb and a lower signal at 11 kb, while in $ERR\gamma^{+/+}$ (+/+, middle) offspring only the upper band appeared and in the $ERR\gamma^{-/-}$ mice (-/-, right) only the lower band	30
Fig. 5 Absolute values of the genotypic distribution for the $ERR\gamma^{+/+}$, $ERR\gamma^{-/-}$ and $ERR\gamma^{+/-}$ mice at four developmental stages (E16, E18, P1 and P3), revealing postnatal underrepresentation of the $ERR\gamma^{-/-}$ mice beginning from P1.	32
Fig. 6 Genotypic distribution for the $ERR\gamma^{+/+}$, $ERR\gamma^{-/-}$ and $ERR\gamma^{+/-}$ mice at four developmental stages (e16, e18, p1 and p3) given in percentage, showing postnatal underrepresentation of the $ERR\gamma^{-/-}$ mice beginning from P1.	32
Fig. 7 Scatter diagram of the numeric values of the - eight pro genotype- adult mice body weights, indicating marked absolute body weight reduction of the $ERR\gamma^{-/-}$ mice.	33
Fig. 8 Average adult body weight values of the three genotypes with SEM (n of each genotype =8), revealing the marked weight reduction of the $ERR\gamma^{-/-}$ mice of.....	33
Fig. 9 Average adult body weight values of the three genotypes normalized to the $ERR\gamma^{+/+}$, showing a the 41.4% body weight reduction of the $ERR\gamma^{-/-}$ mice compared to their wildtype littermates.....	34
Fig. 10 Evaluation of the body weight of the $ERR\gamma^{+/+}$ - $ERR\gamma^{-/-}$ littermate-pairs. Depicted are the $ERR\gamma^{+/+}$ body weight values (100%) and the $ERR\gamma^{-/-}$ values normalized.....	34
Fig. 11 Scatter diagram of body weight values of all the mice assessed at five different developmental stages (E16, E18, P1, P3 and P14), showing a body weight reduction of the knockout mice onwards from P1.	36
Fig. 12 Median body weight values of the assessed mice of all three genotypes normalized to the $ERR\gamma^{+/+}$ mice values showing a considerable weight reduction of the $ERR\gamma^{-/-}$ mice beginning from P1.	36
Fig. 13 Scatter diagram of the adult mice vertex-breech-length of the three genotypes (n= 8), showing an overt smaller size of the $ERR\gamma^{-/-}$ mice compared to their $ERR\gamma^{+/+}$ littermates.....	38
Fig. 14 Average adult vertex-breech-length values of the three genotypes with SEM (n of each genotype =8). $ERR\gamma^{+/+}$ mice 8.3 cm (SEM 0.3), $ERR\gamma^{-/-}$ mice 7.2 cm (SEM	38
Fig. 15 Average adult vertex-breech-length values of the three genotypes normalized to the $ERR\gamma^{+/+}$, signifying a marked length reduction of the $ERR\gamma^{-/-}$ mice compared to their $ERR\gamma^{+/+}$ littermates ($ERR\gamma^{+/+}$ vertex-breech length 100%, $ERR\gamma^{-/-}$ 87.3 % and $ERR\gamma^{+/-}$ 97.3%).	39
Fig. 16 Evaluation of the vertex-breech-length of the $ERR\gamma^{+/+}$ - $ERR\gamma^{-/-}$ littermate-pairs. $ERR\gamma^{-/-}$ values normalized to the ones of their $ERR\gamma^{+/+}$ littermates, revealing a reduction in size of all $ERR\gamma^{-/-}$ mice compared to their $ERR\gamma^{+/+}$ littermates.	39
Fig. 17 Scatter diagram of the absolute vertex-breech-length values of all the mice at five developmental stages (E16, E18, P1, P3 and P14), showing a clear growth delay of the $ERR\gamma^{-/-}$ mice postnatally.....	41
Fig. 18 Median vertex-breech-length of all assessed mice of the three genotypes at five.....	41
Fig. 19 Median vertex-breech-length values of the assessed mice of all three genotypes normalized to the $ERR\gamma^{+/+}$ mice values with the $ERR\gamma^{-/-}$ mice exhibiting growth delay from p 1.....	42

Fig. 20 Adult duplet, $ERR\gamma^{+/+}$ and $ERR\gamma^{-/-}$ (arrow). The $ERR\gamma^{-/-}$ mouse (arrow) has a reduced body weight (average adult $ERR\gamma^{-/-}$ body weight 58.6% of the average $ERR\gamma^{+/+}$ value) and size (average adult $ERR\gamma^{-/-}$ vertex-breech-length 87.3% of the average $ERR\gamma^{+/+}$ value) and outspread hindlimbs at rest.	44
Fig. 21 Genotypic littermate triplet of mice at the age of p14. The $ERR\gamma^{-/-}$ mouse can be differentiated from it's littermates by its reduced body weight (at p14 mean $ERR\gamma^{-/-}$ body weight = 3.1 grams, mean $ERR\gamma^{+/+}$ body weight = 8.0 grams) and size (at p14 mean $ERR\gamma^{-/-}$ vertex-breech-length = 3.3cm, mean $ERR\gamma^{+/+}$ vertex-breech-length = 4.8cm).....	45
Fig. 22 Brains of an adult $ERR\gamma^{-/-}$ and a $ERR\gamma^{+/+}$ littermate pair. The telencephalic cortex of the $ERR\gamma^{-/-}$ is shortened dorsally, with the mesencephalic tegmentum (arrow) protruding to a greater extend between it and the cerebellar region compared to the appearance of the brain of it's heterozygous littermate (asterisk).....	46
Fig. 23 a. Macroscopic appearance of a stomach of a $ERR\gamma^{-/-}$ adult mouse. Note the protruding mass of the gastric corpus (asterisk). b. After a sagittal section a clearer view of the protruding tumorous mass of the inner stomach wall at the level of the corpus (arrow).	46
Fig. 24 Cerebellar cortex, Nissl Staining. The three-layered cortical structure of the cerebellum (stratum moleculare – SM, stratum purkinjiese – SP, stratum granulare – SG) can be seen without any pathological changes. $ERR\gamma^{+/+}$ left, $ERR\gamma^{-/-}$ right.	48
Fig. 25 Hematoxylin Eosin stain of a $ERR\gamma^{+/+}$ (left) and a $ERR\gamma^{-/-}$ (right) stomach. Prominent differences are observed in the $ERR\gamma^{-/-}$ stomach, with epithelial hypertrophy and hyperkeratosis, with formation of keratohyalin bodies and glandular hypertrophy with occasional mononuclear cell infiltration.	49
Fig. 26 Sagittal view of the Substantia nigra Pars compacta and Pars reticulata of the $ERR\gamma^{+/+}$ (left) and the $ERR\gamma^{-/-}$ (right). There were no morphological changes between the two genotypes in the distribution pattern of their long TH-immunoreactive fiber bundles crossing the diencephalon between the thalamic and the subthalamic area reaching the striatum observed.	51
Fig. 28 Average total brain size for the $ERR\gamma^{+/+}$ [7.7 (SEM= 0.51)] and the $ERR\gamma^{-/-}$ [6.2 mm ² (SEM=0.16)] populations with SEM. There is a significant reduction (18.6%) in the $ERR\gamma^{-/-}$ brain size in comparison to the WT. $P < 0.05$	52
Fig. 29 Average values of the size of the telencephalon (TEL) and the telencephalic subregions [the telencephalic cortex (CTX), the telencephalic white matter (TEL WM)	52
Fig. 30 Average values of the size of the mesencephalon (MESENC) and the mesencephalic subregions [the mesencephalic tectum (TCM MES), the mesencephalic tegmentum (TEG MES), the cerebellum (CEREBELLUM), the cerebellar white matter (CEREB. WM.), the cerebellar cortex (CEREB. CTX), the diencephalon (DIENC) and the pons (PONTS) with SEM. Significant differences in size of the assessed regions are shown between the mesencephalon [$ERR\gamma^{+/+} = 1.4 \text{ mm}^2$ (SEM=0.11), $ERR\gamma^{-/-} = 1.2 \text{ mm}^2$ (SEM=0.04)], the mesencephalic tectum [$ERR\gamma^{+/+} = 0.56 \text{ mm}^2$ (SEM=0.02), $ERR\gamma^{-/-} = 0.45 \text{ mm}^2$ (SEM=0.02)], the cerebellum [$ERR\gamma^{+/+} = 1.1 \text{ mm}^2$ (SEM=0.1), $ERR\gamma^{-/-} = 0.75 \text{ mm}^2$ (SEM=0.07)], the cerebellar white matter [$ERR\gamma^{+/+} = 0.13 \text{ mm}^2$ (SEM=0.01), $ERR\gamma^{-/-} = 0.07 \text{ mm}^2$ (SEM=0.001)] and cortex [WT= 0.94 mm ² (SEM=0.1), $ERR\gamma^{-/-} = 0.67 \text{ mm}^2$ (SEM=0.07)] and the pons [$ERR\gamma^{+/+} = 0.51 \text{ mm}^2$ (SEM=0.03), $ERR\gamma^{-/-} = 0.4 \text{ mm}^2$ (SEM=0.02)]. (*) $P < 0.05$	53
Fig. 31 Genotypic differences in brain region size between the $ERR\gamma^{+/+}$ and the $ERR\gamma^{-/-}$ littermate mice. The average values of the brain regions normalized to the genotype's total brain size for the $ERR\gamma^{+/+}$ and $ERR\gamma^{-/-}$ populations with SEM are shown. Regions showing significant differences in size (*) are the mesencephalic tegmentum (11.35% [SEM= 0.56] for the $ERR\gamma^{+/+}$ and 12.32% [SEM=0.46] for the $ERR\gamma^{-/-}$), the cerebellum (14% [SEM=0.39] for the $ERR\gamma^{+/+}$ and 12.03% [SEM=0.73] for the $ERR\gamma^{-/-}$) and the cerebellar cortex (12.16% [SEM=0.16] for the $ERR\gamma^{+/+}$ and 10.92% [SEM=0.81] for the $ERR\gamma^{-/-}$). $P < 0.05$ between groups.....	54

Index of Tables

<i>Table 1</i> A proposed nomenclature for the nuclear receptors. [Table from “A unified nomenclature system for the nuclear receptor superfamily” (4)]	9
<i>Table 2</i> Phylogenetic tree and schematic structure of orphan nuclear receptors present in human, mouse and rat [from Benoit et al. (15)]	12
<i>Table 3</i> Known ERR functions and associated genes [from Tremblay and Giguere (33)].	14

Acknowledgment

This doctoral thesis was my first encounter with fundamental neuroscientific research. The beginning of it all took place after my initial encounter with Professor Dietrich Lorke of the Anatomy Institute who accepted me to be his doctoral candidate. His sharp understanding over the currents of the neuroanatomical world guided me through the first years of the project completion, namely the experimental part and taught me how to be more of a scientist, than just an enthusiastic student.

I also deeply thank Dr. Irm Hermanns-Borgmeyer, who also trusted me to work with her fascinating knockout mouse model and despite my inexperience, always treated me with respect and reassured me, that I could pull this work through.

When I think of the experimental part of the work I need to thank Ms Dagmara Niedzielska, who not only helped me with the animal perfusion procedure on her free weekends, but also took care of me during that period. Ms Cornelia Burger and Ms Susane Feldhaus both from the Anatomy Institute were also a great assistance during this procedure, since without the skillful hands of the first one and the demanding discipline of the latter, I would need endless time to complete my experimental part. Mr. Klaus Siebert also from the Anatomy Institute, was always there for me with exquisite knowledge on staining techniques, not only concerning their application but also in providing me with needful knowledge on their scientific value.

From a clinical point of view, the comments and help of PD Dr. Tim Magnus and Dr. Chi-un Choe from the group of experimental neuroimmunology, propelled me to gain a clear understanding of my results during the discussion part.

In the very end this entire project has been under the supervision of Professor Udo Schumacher, who not only provided me with everything I required, but also supported me morally to continue the project even on difficult times. His saying, “Where is the beef Mr. Ganos?” will accompany me for the rest of my years in scientific works and in my social interactions. I can therefore assure my Professor, that I now know the difference between a hedgehog and a fox and I can accurately spot the beef when there is one.

ABSTRACT

Introduction: The family of orphan nuclear receptors comprises ligand-independent intracellular and/or intranuclear transcription factors, which play several roles in basic physiological functions including cell metabolism, differentiation and growth. The last orphan nuclear receptor identified was the estrogen-related receptor (ERR) γ . Its role in determining morphological and phenotypical properties was examined in the present study using knockout mice.

Materials & Methods: Tissues of ERR $\gamma^{-/-}$ mice generated from embryonic stages to adulthood were histologically analysed after genotypic analysis. Immunohistochemistry was also used. Morphometric analysis was employed to quantify the total and regional brain size of the phenotypes.

Results: We found that ERR $\gamma^{-/-}$ were underrepresented in the postnatal phase indicating to an increased lethality of the phenotype allowing only <1% of the mice to reach adult age. A significant reduction in body weight (41.2% for adult mice) beginning from P1 was observed and a reduction in vertex-breech length (12.7% for adult mice) was noted in the surviving mice. The mice demonstrated dystonic hind-limb reactions leading to tremorous circling body movements (waltzing) and retropulsion. On gross morphological organ examination, the brain and the stomach were altered. The telencephalic region of the ERR $\gamma^{-/-}$ brain was dorsally shortened, with the lamina quadrigemina protruding to a greater extent between the telencephalon and the cerebellum. The mesencephalic tegmentum of the ERR $\gamma^{-/-}$ mice was significantly larger and the cerebellum smaller (normalized values to the absolute brain size of each genotype) compared to their wildtype and heterozygous littermates. The wall of the stomach of the ERR $\gamma^{-/-}$ mice was thickened with protruding bulgy masses, representing glandular hypertrophy with mononuclear cell infiltration.

Conclusions: These results support the hypothesis that the ERR γ receptor plays a key role in neurogenesis and neuronal migration, leading to regional brain disproportionality causing a morphological and functional disruption between the cerebellum and the basal ganglia. They also highlight the suppressive effect of ERR $\gamma^{-/-}$ on cell proliferation in the stomach leading to glandular hyperplasia if absent.

PERSONAL INFORMATION

Name: **Ganos, Christos**

Sex: Male

Marital status: Single

Nationality: Greek

Date of birth: 25.01.82

Place of birth: Thessaloniki, Greece

Address: Wiesinger Weg 7, 20253 Hamburg, Germany

E-mail: cganos@uke.de, cganos@gmail.com

STUDIES

Medical Degree 2008 [University Medical Clinic Eppendorf, Hamburg]

Doctoral Thesis [2005 – current] “The characterization of the ERR-gamma” at the Department of Experimental Anatomy [Working Group: Developmental Neuroanatomy] and the Center for Molecular Neurobiology [ZMNH] of the University of Hamburg in Germany.

Currently, while undergoing the period of neurological specialization scientifically working on the characterization of a family with a novel SCA14 Mutation under the supervision of Prof. Alexander Muenchau.

FELLOWSHIPS - AWARDS

Nominee for the international Lindau Meeting 2008

Teacher of the Year Award 2008/2009 at the University Medical Center Eppendorf, Hamburg

LANGUAGES

English (fluent)

German (fluent)

Greek (native)

Bulgarian (fluent)

Japanese (basic)

TEACHING

Movement Disorders and Neurodegeneration to undergraduate medical students.

SCIENTIFIC INTERESTS

Neurodegeneration (Parkinsonian Syndroms, Hereditary Ataxias), Tourette’s syndrome.

MISCELLANEOUS

Art Critic for the NY Arts Magazine (2007 – 2008) and various other artistic/lifestyle Magazines.

POSTERS

1. “Characterization of the Estrogen-Related Receptor gamma deficient mice. The last of the orphan nuclear receptors implicated in neuronal development, cell metabolism and proliferation”, at the annual national neurological congress of the German Society of Neurology (“DGN”) in Nuerneberg, September 2009.

EIDESSTATLICHE VERSICHERUNG

Ich versichere ausdrücklich, dass ich die Arbeit selbständig und ohne fremde Hilfe verfasst, andere als die von mir angegebenen Quellen und Hilfsmittel nicht benutzt und die aus den benutzten Werken wörtlich oder inhaltlich entnommenen Stellen einzeln nach Ausgabe (Auflage und Jahr des Erscheinens), Band und Seite des benutzten Werkes kenntlich gemacht habe.

Ferner versichere ich, dass ich die Dissertation bisher nicht einem Fachvertreter an einer anderen Hochschule zur Überprüfung vorgelegt oder mich anderweitig um Zulassung zur Promotion beworben habe.

Unterschrift: